Check for updates

Anionic fructose-related conformational and positional isomers assigned through PES experiments and DFT calculations†

Zhen Zeng and Elliot R. Bernstein (ID) *

Gas phase, isolated fructose anionic species, fructose⁻, (fructose-H)⁻, (fructose-OH)⁻, and (fructose-H₂O)⁻, are investigated employing anionic photoelectron spectroscopy (PES) combined with density functional theory (DFT) calculations. The PES vertical detachment energies (VDEs) for these anions are determined and, based on these experimental values, their calculated anionic structures are assigned. Generation of these four species through the matrix assisted laser desorption ionization (MALDI) process is sample desorption substrate dependent. The parent anion fructose⁻ exists as a single, dominant open chain structure in the gas phase, with substrate dependent specific conformational isomers. (Fructose-H)⁻ and (fructose-OH)⁻ are mainly produced from the laser ablation process rather than from fragmentation reaction pathways associated with the parent anion species. Both conformational and positional isomers are identified in the gas phase for these latter anions. (Fructose-H₂O)⁻ has two types of positional isomers, both of which contribute to two different components of the observed PES feature. The fixed positions for losing an OH group and an H atom, in addition to thermodynamic calculations, provide reaction pathways for generating a dehydration product (open chain structures) from the parent anion (open chain and furanose structures), further demonstrating the active nature of fructose upon capturing an extra electron.

I. Introduction

Polysaccharides, formed by the union of three or more monosaccharide molecules, play important roles in biological cell structure and function. Among these are starch acting as a food storage material, peptidoglycans in cell walls, cellulose in plant cell walls, and glycogen serving as a form of energy storage. Disaccharides, for instance sucrose found in many plants, lactose found in milk, and mannose serving in human metabolism, are important nutritional supplements in the human body. Monosaccharides are also important for structural frameworks of nucleosides: they can bind with proteins and/or lipids to form glycosylated derivatives. Conformational behavior and fragmentation mechanisms of monosaccharides can provide important insight into their roles as structural components, as energy storage and release species, and as constituent building blocks with other molecules in biological cells.

Because carbohydrates have low vapor pressure and are thermally unstable, generation of intact molecular ions for study under isolated conditions has been difficult. Since the 1980s, considerable research has been focused on the mass spectroscopic investigation of sugars with the goals of elucidating their fragmentation patterns and obtaining their fragmentation mechanisms.[1–6] The different ionization techniques employed include field desorption,[7–9] electrospray ionization (ESI),[2,6,10] fast atom bombardment (FAB),[11–13] chemical ionization,[14,15] liquid secondary ion mass spectrometry (LSIMS),[16,17] infrared multiple-photon dissociation (IR-MPD),[18] vacuum/extreme ultraviolet photoionization (VUV/EUV),[19,20] laser desorption,[4,5] and matrix assisted laser desorption ionization (MALDI).[1,3,21–23] Concurrently, isotopic labeling has been employed to identify fragmentation sites of a sugar target molecule, thereby avoiding ambiguous stoichiometric assignments. MALDI is the most common strategy for the study of metastable fragmentation anions of deprotonated monosaccharides,[22,24] which suggests that MALD ionization processes generate target parent anions with *ca.* 4 eV internal energy from which deprotonation can occur.[22] Site selective fragmentations have been explored with the aid of dynamics simulation.[24,25]

Conformational characterizations are less easily and uniquely determined. Within the last 15 years,[26] gas phase laser spectroscopy has been established as a prolific source for the investigation of sugar conformational preferences and molecular recognition for substituted saccharides. Such studies

Department of Chemistry, NSF ERC for Extreme Ultraviolet Science and Technology, Colorado State University, Fort Collins, CO 80523, USA. E-mail: erb@colostate.edu
† Electronic supplementary information (ESI) available: Low lying isomers of fructose⁻, (fructose-H)⁻, (fructose-OH)⁻, and (fructose-H₂O)⁻ as well as their corresponding neutrals. See DOI: 10.1039/c7cp03492j

This journal is © the Owner Societies 2017

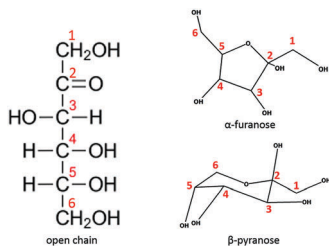*Phys. Chem. Chem. Phys.*, 2017, **19**, 23325–23344 | 23325

Fig. 1 Schematic structures of D-fructose with C atom numbering.

include mass selected vibrational spectroscopy employing a double resonance laser IR-UV ion dip, UV-IR and UV-UV hole burning spectroscopy for isolated neutral saccharides,[27–35] and IRMPD studies of charged saccharides.[18,36–39] Microwave spectroscopy for biologically relevant neutral monosaccharides has recently been reported as well, including ribose,[40] fructose,[41,42] 2-deoxy-D-ribose,[43] galactose,[44] and glucose.[45] These studies imply that specific conformers can be identified for these neutral isolated saccharides through high resolution microwave and theoretical approaches.

Free neutral fructose (see Fig. 1) has been studied in the gas phase through ultrafast UV laser vaporization combined with Fourier-transform microwave spectroscopy.[41] A full structural determination of free fructose was made. Neutral fructose exists in isolation as a β-pyranose, conformationally locked structure. Additionally, other two broad-band chirped-pulsed Fourier transform microwave spectroscopy studies of neutral fructose further distinguish two conformers for β-D-fructo-pyranose as different rotamers.[42,46] Fragmentation of deproto-nated D-fructose has also been investigated.[24] In this latter study, theoretical simulations of the observed reactions suggest that reaction steps include intramolecular proton transfer, ring opening at the anomeric C–O bond, and antiperiplanar dissociation.

A dissociative electron attachment (DEA) study of fructose and other two similar molecules, furan (FN) and tetrahydro-furan (THF), has been carried out. Both FN and THF are found to be weak electron scavengers. Unlike FN and THF, upon low energy electron interaction, fructose incurs complex decom-position reactions in an anionic form, for example, via loss of one, two, or three water units.[47]

Studies of the conformation, stability, and fragmentation mechanisms for anionic sugars facilitate and enable elucidation of secondary low energy electron radiation damage mechanisms for DNA and RNA in cellular systems. For example, experimental DEA investigation of thymidine suggests that the sugar unit can capture a low energy electron, leading to subsequent fragmenta-tion at the rupture of the N1–C1 bond between the thymine and the sugar moiety.[48] Further DEA experiments for deoxyribose and D-ribose,[49,50] components of DNA and RNA, respectively, reveal that very low energy electron attachment induces decomposition of the anions with loss of one or two water molecules, as well as small carbon containing neutral moieties. These results further support the idea that the sugar moiety is an active site for DNA single-strand breaks at a molecular level. Employing DEA to study

the fragmentation of anionic monosaccharides provides ion formation mechanisms, including reaction schemes involving the transient parent anion formed upon electron capture. The parent anion can then in principle generate the fragmented daughter anions detected specifically.

For investigation of the electronic and geometric structures of anionic isolated, unsubstituted monosaccharides, anionic photoelectron spectroscopy (PES), coupled with density func-tional theory (DFT) calculations, is an essential and productive approach. Individual isolated sugar molecules can be studied without interaction with their environment or substituents; therefore, structural assignment provides a benchmark for understanding a sugar molecule's role both as a structural component and a stored energy carrier. Moreover, interactions with other molecules in a biological cell can be ascertained without additional environmental perturbations or interferences.

In the present work, we conduct PES experiments and DFT calculations on gas phase, isolated fructose related anionic species. The isolated fructose parent anion and related species are explored, and both their electronic and geometric structures (conformational and positional) are revealed through comparison of experimental and calculated VDEs. Conformational isomers have different geometries but the same positions for loss of one H atom or OH group. Positional isomers have different fragmented moiety positions but with similar conformations. Structures can then be assigned based on the agreement between calculated and observed VDEs. Parent anion species are observed employing MALDI techniques. The intensity of the parent anion and related fragment species of fructose is dependent on the MALDI sample desorption substrates. Formation mechanisms for fructose⁻, (fructose-H)⁻, (fructose-OH)⁻, and (fructose-H$_2$O)⁻ are calculated and identified.

II. Experimental procedures

The experimental apparatus consists of three parts: a pulsed supersonic nozzle with an attached matrix assisted laser desorption ionization (MALDI) source, a reflectron time of flight mass spectrometer (RTOFMS), and a magnetic bottle photoelectron TOF spectrometer (MBTOFPES). Details of this system (RTOFMS/MBTOFPES) can be found in our previous publications.[51,52] The nozzle employed for the sample beam generation is constructed from a Jordan Co. pulsed valve and a laser desorption attachment. All sample drums for the MALDI are prepared by wrapping different sample desorption substrates (filter paper, Cu, Ti, Al, Zn, or Au) on a clean Al drum.[53] A mixed solution of D-fructose and matrix (R6G or DCM) dye with a mole ratio of ~3:2 in a solvent (typically, methanol or acetonitrile) is uniformly sprayed on the drum/substrate surface using an air atomizing spray nozzle (Spraying System Co.) with a siphon pressure of 10 psig. During the spraying process, the sample drum is rotated under heat of a halogen lamp in a fume hood to ensure that deposition of D-fructose and matrix on the drum surface is homogeneous and dry. The well-coated and dried sample drum is then placed in the laser ablation head/nozzle assembly and put

into the vacuum chamber. Second harmonic (532 nm) light pulses from a Nd:YAG laser are used to ablate the sample drum, which rotates and translates simultaneously to maintain a fresh sample area for each laser ablation pulse. Whole D-fructose molecules are desorbed from the drum, interact with other species (including electrons) in the ablated material plume, are entrained in the supersonic flow of helium carrier gas with a 50 psi backing pressure through a 2×60 mm channel in the ablation head, and expanded into the sample chamber. With a closed pulsed valve, the RTOFMS chamber pressure is $\sim 6 \times 10^{-8}$ Torr. Generated molecular anions are pulsed into the RTOFMS and are mass analyzed using the RTOFMS. For PES experiments, specific anions are first mass selected and decelerated before interacting with a 355 nm (3.496 eV), or 266 nm (4.661 eV) laser beam from another Nd:YAG laser in the photodetachment region. Photodetached electrons are collected and energy analyzed by the MBTOFPES at nearly 100% efficiency. The photo-detachment laser is operated at a 10 Hz repetition rate, while the ablation laser is synchronously triggered at 5 Hz. Data are collected at 5 Hz employing a background subtraction with alternation of the ablation laser on/off if the detachment laser generates 266 nm or higher energy photons. Every photo-electron spectrum is calibrated by the known spectra of Cu^- at the employed detachment photon energy. The photoelectron energy resolution is $\sim 4\%$ (40 meV for 1 eV kinetic energy electrons), as anticipated for a 1 m PES flight tube.

III. Computational methods

For computationally large organic neutral molecules and molecular anions, such as saccharides (*e.g.*, fructose $C_6(H_2O)_6$ and ribose $C_5(H_2O)_5$), one must explore the various available computational algorithms to determine which approximate method will best predict experimental results efficiently, reproducibly, and reliably. The main point of performing spectroscopy of any kind on such systems is to theoretically validate the derived physical properties (*e.g.*, structures, energy levels, electron affinities, vertical electron detachment energies...) that can be or have been measured experimentally; thereby, with good agreement between the calculated and experimental results, properties that have not or cannot be directly measured can be reliably estimated and predicted. Thus, irrespective of the determined method of calculation, one must justify the results of any calculation based on what properties can be mutually obtained by both theory and experiment. The present theoretical studies are evaluated and justified for fructose isolated molecule and molecular anions through the best agreement for VDEs between predictions and observations. We begin this approach by first considering which algorithms have been reported in the past to generate best structures and spectroscopic information, in general, for neutral saccharides and their related anionic species.

Calculational studies of sugar molecular anions are rare. Long range corrected DFT methods are typically employed to study the dissociative excess electron attachment mechanism

to biomolecules[54,55] such as ribose and fructose. A B3LYP functional with a DZP++ basis set has been used to predict geometries, energies, and charge distributions of both neutral and anionic 2'-deoxyribonucleosides.[56] Through DFT B3LYP/6-311++G(d,p) calculations, experimental VDEs for anionic 2'-deoxycytidine homodimers can be well assigned to particular structures.[57] A recent theoretical study on unstable organic anionic species compares various density functionals, as well as CCSD(T):[58] it finds that functionals B3PW91 and M06 are the best ones for generating properties of such anions, and that additionally B3LYP and PBE0 reproduce correct observed behavior. Ref. 58 also suggests that care must be taken with MP2 and CCSD(T) algorithms to employ a sufficiently large basis set. The B3LYP functional, coupled with a basis set having diffuse functions, has been widely used to evaluate the electron affinities (EAs) or VDEs of organic molecules, especially DNA or RNA bases,[59,60] and their related anionic nucleic acid related species.[61,62] The usefulness of the B3LYP functional for the prediction of extra electron binding energies has been reviewed: it can provide excellent EAs for valence bound molecular anions.[63] Based on our former anionic energetic materials studies, the B3LYP/6-311++G(d,p) level of theory is both reliable and predictive for their electronic properties and reactions, as demonstrated through good agreement with experimental results.[64]

DFT (B3LYP and M062X) and MP2 methods with a 6-311++G(d,p) basis set are extensively employed for calculations of gas phase sugar neutrals.[27,28,40,41,65,66] MP2 and M062X give relatively consistent results for saccharide neutrals and the MP2/6-311++G(d,p) level of theory represents an effective compromise algorithm for structures and transition energies determined by microwave spectroscopy.[41] The M062X functional can be a good DFT alternative to MP2 considering both accuracy and computational cost.

Given the above literature precedents and our own experience with CASSCF, CASMP2, DFT, and MP2 calculations for energetic molecules,[67] all calculations are executed using density function theory (DFT) employing Becke's three-parameter hybrid (B3LYP)[68–70] functional and a 6-311++G(d,p) basis set for all atoms, as implemented in the Gaussian 09 program.[71] The low energy isomers for every species are reoptimized employing the M062X[72,73] functional with the same basis set. The MP2 method and the APFD[74] functional with the same basis set are also chosen for further examination of several typical isomers of the fructose related species. No symmetry restrictions are applied for the calculations. Optimization of the low lying isomers for each anion and neutral is performed with harmonic vibrational frequencies calculated to confirm that the obtained structures are the true local minima. Theoretical VDEs for each anionic species are calculated as the energy difference between the ground state of the anion and its corresponding neutral at the same structure as the anion. The optimizations of neutrals are also conducted with anionic structures as the initial structures by removal of the extra electron. The lowest energy anions will not necessarily give rise to the lowest energy neutrals and the optimized neutrals are not necessarily directly correlated with the observed experimental VDEs. For further electronic

structure based understanding of the observed fructose related species behavior, a Natural Bond Orbital (NBO) analysis is performed based on the B3LYP functional and the same basis set.

IV. Experimental results

By changing different sample desorption substrates, four fructose related gas phase, anionic species are identified: fructose$^-$, (fructose-H)$^-$, (fructose-OH)$^-$, and (fructose-H$_2$O)$^-$. Concentrations of these anions and their various positional and conformational isomers are substrate dependent. Five sample desorption substrates, filter paper, Cu, Ti, Al, and Zn, with a DCM matrix, all give rise to (fructose-H)$^-$ and (fructose-H$_2$O)$^-$ anions. A Zn substrate (some surface Zn$_5$(OH)$_6$(CO$_3$)$_2$) generates highest intensity (fructose-H)$^-$ and (fructose-H$_2$O)$^-$ ions. The parent anion fructose$^-$ is readily observed with both Al (Al$_2$O$_3$) and Zn substrates, but with different conformational constituents. The fructose$^-$ anion is not observed with either a filter paper or a Cu substrate. (Fructose-OH)$^-$ is only observed when employing an RG6 matrix with a Cu substrate. An Au substrate is also considered; however, no uniquely identifiable parent anion or fragment species can be observed with an Au metal surface coupled with the MALDI process. Therefore, a Zn substrate with a DCM matrix is chosen to generate fructose$^-$, (fructose-H)$^-$, and (fructose-H$_2$O)$^-$ specific ions, and a Cu substrate with an R6G matrix is chosen to generate the (fructose-OH)$^-$ anion. The mass spectrum showing anionic fructose$^-$, (fructose-H)$^-$, and (fructose-H$_2$O)$^-$ is presented in Fig. 2. The mass spectrum of anionic (fructose-OH)$^-$ is presented in Fig. 3 (left).

VDEs are measured from the maxima of the corresponding PES peaks. The photoelectron spectrum of fructose$^-$, recorded using 355 nm photons and a Zn substrate, is presented in Fig. 4 (left), which shows a broad peak. The photoelectron spectrum of fructose$^-$ generated through an Al substrate is also displayed in Fig. 4 (right), showing a narrower peak centered at $\sim$1.93 eV. The left spectrum displays not only the similar feature as the right spectrum but also a shoulder peak centered at $\sim$1.58 eV, corresponding to different isomers. The photoelectron spectrum of (fructose-H)$^-$ using 266 nm photons is displayed in Fig. 5, revealing a broad peak centered at $\sim$3.44 eV, within the range from $\sim$3.44 eV to $\sim$4.34 eV. The shoulder at the lower electron binding energy (EBE) portion of this feature may also contain vibrational hot bands, corresponding to transitions from vibrationally excited states of the anion ground electronic state to electronic ground states of the isomeric neutrals. The photoelectron spectra of (fructose-H$_2$O)$^-$ recorded with 355 and 266 nm photons are presented in Fig. 6, showing two distinguishable components centered at $\sim$1.55 and $\sim$2.13 eV. Fig. 3 (right) shows the photoelectron spectrum of (fructose-OH)$^-$ using 266 nm photons, revealing a very broad peak centered from 2.62 eV to above 4 eV. The experimental VDEs of fructose$^-$, (fructose-H)$^-$, (fructose-OH)$^-$, and (fructose-H$_2$O)$^-$ are summarized in Table 1.
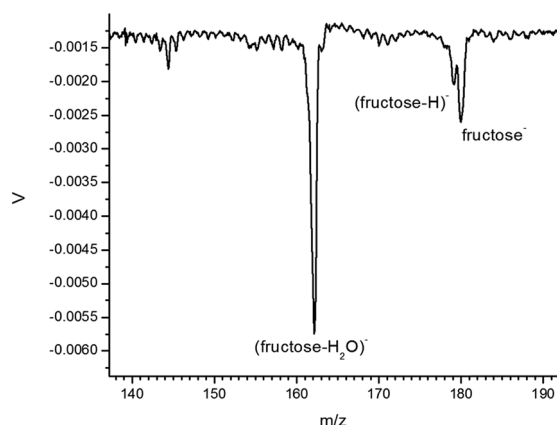
V. Theoretical results

Sugar molecules have a great number of molecular geometries owing to the flexible OH group rotation, C–C bond rotation,
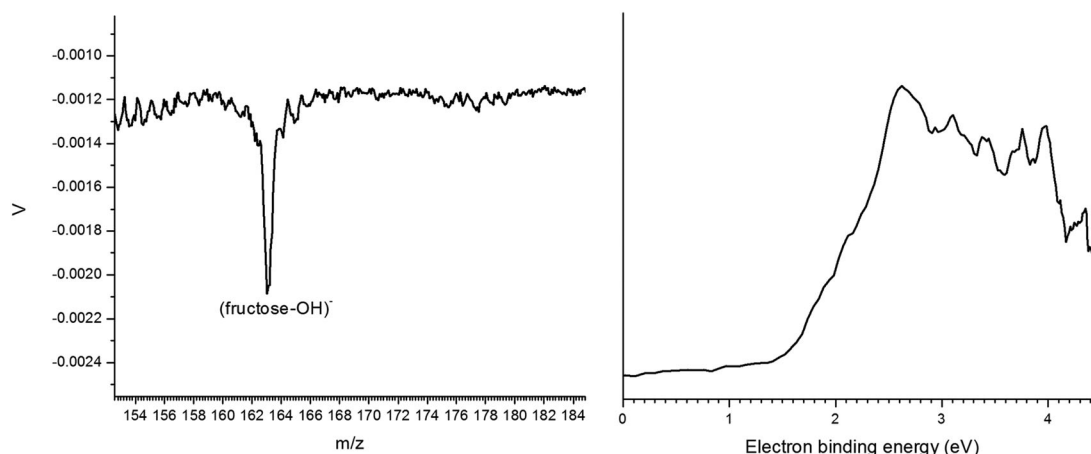

Fig. 2 Mass spectrum of fructose with sample (D-fructose/DCM) sprayed on a Zn surface.

Fig. 3 Mass spectrum of (fructose-OH)$^-$ (left) and photoelectron spectrum of (fructose-OH)$^-$ recorded with 266 nm photons (right) with sample (D-fructose/R6G) sprayed on a Cu surface.

23328 | *Phys. Chem. Chem. Phys.*, 2017, **19**, 23325–23344
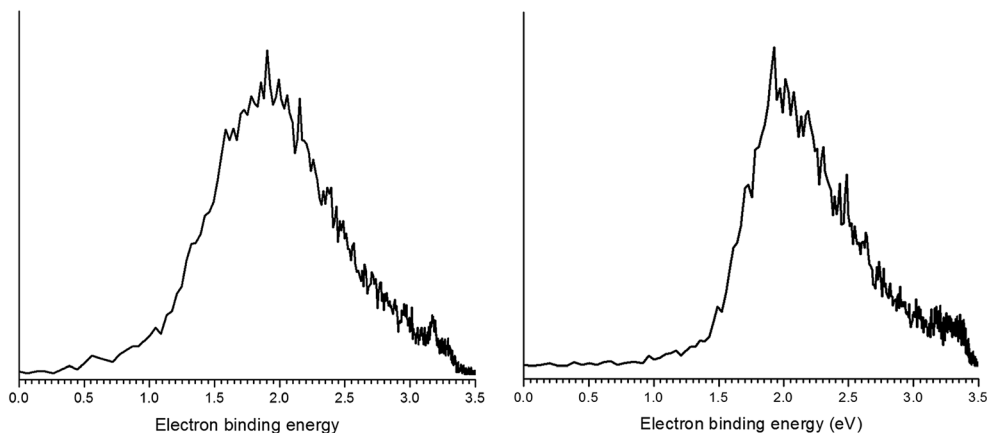
This journal is © the Owner Societies 2017

Fig. 4 Photoelectron spectra of fructose⁻ recorded with 355 nm photons with sample (D-fructose/DCM) sprayed on a Zn surface (left) and Al surface (right).
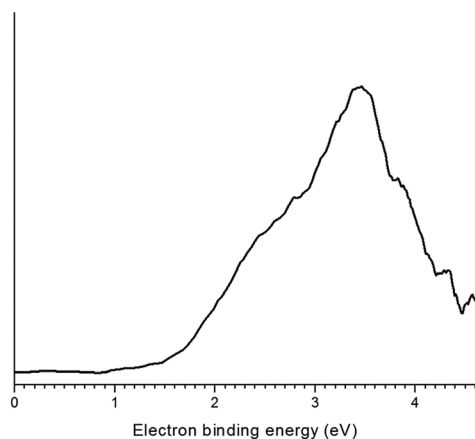

Fig. 5 Photoelectron spectrum of (fructose-H)⁻ recorded with 266 nm photons with sample (D-fructose/DCM) sprayed on a Zn surface.

as well as diverse intramolecular hydrogen bonding configurations. Loss of H/OH moieties has many different possibilities. Theoretically based assignments for the experimental spectra concentrate on open chain and cyclic (pyranose and furanose) structures, but not on the specific orientation of OH groups, which are arranged specifically for the chosen fructose parent molecule.

The low lying isomers of fructose related species are first optimized using the B3LYP/6-311++G(d,p) level of theory. The lower lying isomers of fructose⁻, (fructose-H)⁻, (fructose-OH)⁻ and (fructose-H$_2$O)⁻ are then reoptimized *via* the M062X/6-311++G(d,p) approach based on the initial B3LYP structures. The calculated VDEs of every specific isomer for each species generated by these two functionals are close to each other, as can be seen in Table 1. For the fructose⁻ parent anion, as shown in Table 1, Fig. 7 and Fig. S25 (ESI†), both theoretical methods show nearly identical lowest energy isomers with the calculated VDEs in accordance with the experimental results. The other structures optimized from both approaches are also similar, but with a slightly different energy order, especially for higher energy cyclic structures. For (fructose-H$_2$O)⁻, as shown in Table 1, Fig. 10 and Fig. S28 (ESI†), both functionals show similar lower energy isomers assigned to contribute to experimental results. For both (fructose-H)⁻ and (fructose-OH)⁻, the two functionals also predict nearly indistinguishable structures with comparable VDEs to the observed broad PES peak, but with a slightly different energy order. The typical isomers (open chain and furanose ring) of fructose⁻ and two positional isomers ((A) and (C)) of (fructose-H$_2$O)⁻ are also optimized and their VDEs are calculated based on MP2/6-311++G(d,p), and APFD/6-311++G(d,p). As shown in Table S1 (ESI†), the VDEs calculated at the MP2 level are smaller by ∼0.3 eV compared to the experimental ones. Results from the APFD functional are in reasonable agreement with the experimental ones. By considering both accuracy and consistency of different functionals, the B3LYP/6-311++G(d,p) level of theory is chosen for interpreting the theoretical calculations.

The low lying isomers of fructose⁻, (fructose-H)⁻, (fructose-OH)⁻, and (fructose-H$_2$O)⁻ anions, as well as their corresponding neutrals, are shown in Fig. 7–10 and Fig. S17–S20 (ESI†). More isomers are presented in the ESI.† Note that the figure numbers in the ESI† are related to those of the text figures, as for example Fig. 7 ⇔ Fig. S7 (ESI†). The calculated VDEs and relative energies of the anions are summarized and compared with the experimental results in Table 1. Although optimized neutral structures are not necessarily directly related to the experimental VDE results, the low lying isomers of neutrals are provided to show their structural characteristics and for comparison with anions.

The typical low lying isomers of the fructose⁻ anion are shown in Fig. 7. The first eight isomers are open chain structural polymorphs,[41] while the remaining four isomers have cyclic structures, including β-pyranose, α-pyranose, α-furanose, and β-furanose. More cyclic structures with different polymorphs have higher relative energies and are shown in Fig. S7 (ESI†). Isomers fructose⁻ (A) and fructose⁻ (B) have similar open chain structures but with different (6)OH group orientations. The calculated VDE of isomer (A) is 1.87 eV, in good agreement with the experimental observations (1.93 eV) at the higher electron binding energy part of the experimental feature (see Fig. 4).
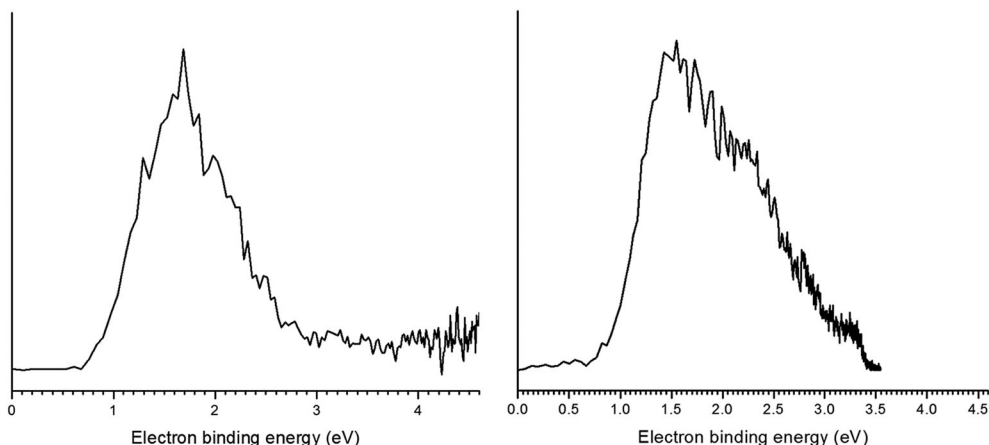
Fig. 6 Photoelectron spectra of (fructose-H_2O)$^-$ with sample (D-fructose/DCM) sprayed on a Zn surface recorded with 266 nm photons (left) and 355 nm photons (right).

Isomer (B) has a relative energy of 0.35 eV with respect to isomer (A) and a calculated VDE of 1.57 eV, which is consistent with the measurement (1.58 eV) of the lower electron binding energy shoulder of the experimental spectrum derived from sample ablation on a Zn substrate. The isomer fructose$^-$ (C) has similar geometry to that of isomer (B) but with different (5)OH group orientations: its relative energy is 0.39 eV and the calculated VDE is 1.46 eV, close to the experimental one (1.58 eV). The isomer fructose$^-$ (D) has a calculated VDE of 1.02 eV, significantly lower than the experimental values, and thus it is not likely to be present in our experiments. Its relative energy is $\sim$0.50 eV. The remaining isomers have higher energies (above 0.50 eV) than the lowest lying open chain isomer (A). Cyclic conformations all have very low electron binding energies. Obviously, isomer (A) mainly contributes to the higher energy component features centered at 1.93 eV in both spectra with different substrates. The lower electron binding energy part in the spectrum of fructose$^-$ employing a Zn substrate can be mostly related to isomer (B). Isomer (C) can also exist in the experiments to contribute to the lower EBE part of the observed composite PES feature. The ground state of neutral fructose includes both open chain and pyranose structures nearly degenerate in energy, as depicted in Fig. S17 (ESI†).

As will become clear below, all fructose related PES features are composed of a collection (superposition) of energy available isomers with appropriate values for VDEs. One can thus exclude isomers for a comparison between calculated and observed VDEs that have calculated VDEs outside the observed PES feature width. As mentioned above, fructose$^-$ (D) has a calculated VDE of 1.02 eV, a value not present within the experimental PES line shape. Additionally, since the anionic fructose$^-$ (D) isomer has a $\Delta E > 0.5$ eV (0.25 eV $\sim$ 2000 cm^{-1} $\sim$ 3000 K), it would not be expected to be present in the experimental beam. Based on a generalization of these results, one can justifiably exclude isomers from this comparison that are higher in energy than $\sim$0.5 eV above the lowest energy calculated isomer. Structures with relative energy $>$0.50 eV are nonetheless shown for comparison with the lower energy isomers in Fig. 7–10. Also note, from the above

discussion, that isomers derived from fructose$^-$ (D) are probably not in the experimental sample.

For the calculation of the electronic and geometric structures of the fructose$^-$ anion, the approach, as outlined above, is to determine the best, low energy neutral fructose structures to which an electron can then be added: these new anionic species are then re-optimized for the identification of low energy structures of the fructose$^-$ anion with acceptable (experimental) VDEs. This approach becomes more problematic as fragmented ((fructose-X)$^-$, X = H, OH, H_2O) anions are considered, because choosing an appropriate reactant and product species implies a choice of reaction mechanism for the fragment. Moreover, a given reaction mechanism can involve either kinetic or thermodynamic issues. These considerations have implications for calculating the VDE of a particular isomer. The approach taken for these isomer determinations for each (fructose-X)$^-$ fragment anion is a hierarchical one, in which a number of less fragmented calculated stable species are chosen to generate the more fragmented stable species. Different pathways are also considered as possible starting points for the calculations (e.g., various neutral reactants). The guiding principle for these theoretical studies is to obtain experimental VDEs and EAs based on a given isomeric anionic structure. The neutral structure derived from this initial starting anionic isomeric structure may not necessarily be one of the lowest energy structures for the respective species generated by PES, even if the initial anionic structure is the lowest energy anion one for that species.

For geometrical optimization of (fructose-H)$^-$, fructose$^-$ open chain isomers (A), (B), (C), the lowest energy pyranose isomer (I), and the lowest energy furanose isomer (K) are chosen to be the initial structures followed by loss of an H atom at different possible positions. The subsequent low lying isomers of (fructose-H)$^-$ are shown in Fig. 8. The most stable isomer (A) of (fructose-H)$^-$ derives from open chain fructose$^-$ (C) through loss of an H atom from the oxygen on (3) position ((3)H). Its theoretical VDE is calculated to be 4.00 eV, in the range of the experimental observation ($\sim$3.44 eV to $\sim$4.34 eV). The isomer (fructose-H)$^-$ (B) arises from fructose$^-$ (A) by losing

Table 1 Relative energies (ΔE) of the low energy isomers of fructose$^-$, (fructose-H)$^-$, (fructose-OH)$^-$, and (fructose-H$_2$O)$^-$, and comparison of their calculated VDEs based on B3LYP/6-311++G(d,p) and M062X/6-311++G(d,p) algorithms with experimental measurements. All energies are in eV. The labels in bold indicate the isomers which are assigned to contribute most prominently to the experimental spectra features

		B3LYP/6-311++G(d,p)		M062X/6-311++G(d,p)		
		ΔE	Theo. VDE	ΔE	Theo. VDE	Exp. VDE
Fructose$^-$	**Fructose$^-$ (A)**	0.00	1.87	0.00	1.85	1.93
	Fructose$^-$ (B)	0.35	1.57	0.39	1.52	1.58
	Fructose$^-$ (C)	0.39	1.46	0.44	1.40	
	Fructose$^-$ (D)	0.50	1.02	0.55	1.07	
	Fructose$^-$ (E)	0.54	1.28	0.55	1.23	
	Fructose$^-$ (F)	0.61	0.95	0.46	1.52	
	Fructose$^-$ (G)	0.61	1.21	0.66	1.13	
	Fructose$^-$ (H)	0.75	1.31	0.59	1.27	
	Fructose$^-$ (I)	0.91	0.12	0.57	−0.08	
	Fructose$^-$ (J)	1.00	0.04	0.76	−0.19	
	Fructose$^-$ (K)	1.04	0.16	0.85	0.04	
	Fructose$^-$ (L)	1.10	0.24	0.77	−0.08	
(Fructose-H)$^-$	**(Fructose-H)$^-$ (A)**	0.00	4.00	0.09	4.24	∼3.44 to ∼4.34
	(Fructose-H)$^-$ (B)	0.09	3.91	0.18	4.06	
	(Fructose-H)$^-$ (C)	0.16	4.07	0.00	4.16	
	(Fructose-H)$^-$ (D)	0.27	3.73	0.04	3.94	
	(Fructose-H)$^-$ (E)	0.38	3.50	0.48	3.64	
	(Fructose-H)$^-$ (F)	0.42	3.63	0.17	3.92	
	(Fructose-H)$^-$ (G)	0.51	3.57	0.30	3.63	
	(Fructose-H)$^-$ (H)	0.56	3.74	0.69	3.76	
	(Fructose-H)$^-$ (I)	0.63	3.57	0.37	3.84	
	(Fructose-H)$^-$ (J)	0.69	3.22	0.51	3.30	
(Fructose-OH)$^-$	**(Fructose-OH)$^-$ (A)**	0.00	3.23	0.00	3.34	∼2.62 to ∼4.35
	(Fructose-OH)$^-$ (B)	0.08	3.45	0.13	3.51	
	(Fructose-OH)$^-$ (C)	0.11	3.28	0.00	3.34	
	(Fructose-OH)$^-$ (D)	0.14	3.47	0.05	3.66	
	(Fructose-OH)$^-$ (E)	0.15	2.89	0.15	2.98	
	(Fructose-OH)$^-$ (F)	0.34	3.06	0.33	3.17	
	(Fructose-OH)$^-$ (G)	0.35	3.32	0.37	3.43	
	(Fructose-OH)$^-$ (H)	0.38	3.08	0.29	3.16	
	(Fructose-OH)$^-$ (I)	0.47	2.97	0.33	3.17	
	(Fructose-OH)$^-$ (J)	0.50	2.79	0.55	2.85	
	(Fructose-OH)$^-$ (K)	0.54	3.14	0.52	3.21	
	(Fructose-OH)$^-$ (L)	0.57	3.05	0.54	3.11	
	(Fructose-OH)$^-$ (M)	1.24	2.92	1.23	2.95	
	(Fructose-OH)$^-$ (N)	1.25	2.93	1.22	2.96	
	(Fructose-OH)$^-$ (O)	1.85	2.37	1.52	2.31	
	(Fructose-OH)$^-$ (P)	1.85	2.37	1.52	2.31	
(Fructose-H$_2$O)$^-$	**(Fructose-H2O)$^-$ (A)**	0.00	1.96	0.00	2.02	2.13
	(Fructose-H$_2$O)$^-$ (B)	0.01	1.95	0.02	2.10	
	(Fructose-H$_2$O)$^-$ (C)	0.33	1.48	0.37	1.60	1.55
	(Fructose-H$_2$O)$^-$ (D)	0.34	1.54	0.08	1.67	
	(Fructose-H$_2$O)$^-$ (E)	0.37	1.57	0.29	1.48	
	(Fructose-H$_2$O)$^-$ (F)	0.38	3.39	0.34	3.06	
	(Fructose-H$_2$O)$^-$ (G)	0.70	4.13	0.58	4.19	
	(Fructose-H$_2$O)$^-$ (H)	0.70	4.13	0.58	4.18	
	(Fructose-H$_2$O)$^-$ (I)	1.05	3.77	0.93	2.94	
	(Fructose-H$_2$O)$^-$ (J)	1.05	3.79	0.92	2.94	
	(Fructose-H$_2$O)$^-$ (K)	1.62	3.85	1.05	4.42	

(4)H and has a relative energy of 0.09 eV. The calculated VDE of this isomer is 3.91 eV which agrees with the experimental one. Isomers (fructose-H)$^-$ (C) and (D) develop from pyranose structures by losing (2)H and (3)H, respectively. Their calculated VDEs are 4.07 and 3.73 eV, both in good accordance with the experimentally determined values from the broad PES feature. The isomer (fructose-H)$^-$ (E) loses (3)H from the parent isomer (A). It has a relative energy of 0.38 eV and a theoretical VDE of 3.50 eV, consistent with the experimental feature. The remaining

low lying isomers come from pyranose and furanose cyclic conformations by losing an H atom at different positions. Their calculated VDEs are all in agreement with the experimental determination, but they have higher energies compared to the lowest energy isomer. More isomers are displayed in Fig. S8 (ESI†).

Thus, the broad feature in the photoelectron spectrum of (fructose-H)$^-$ is composed of many isomers, mainly including open chain and pyranose structures. The lower EBE part may be
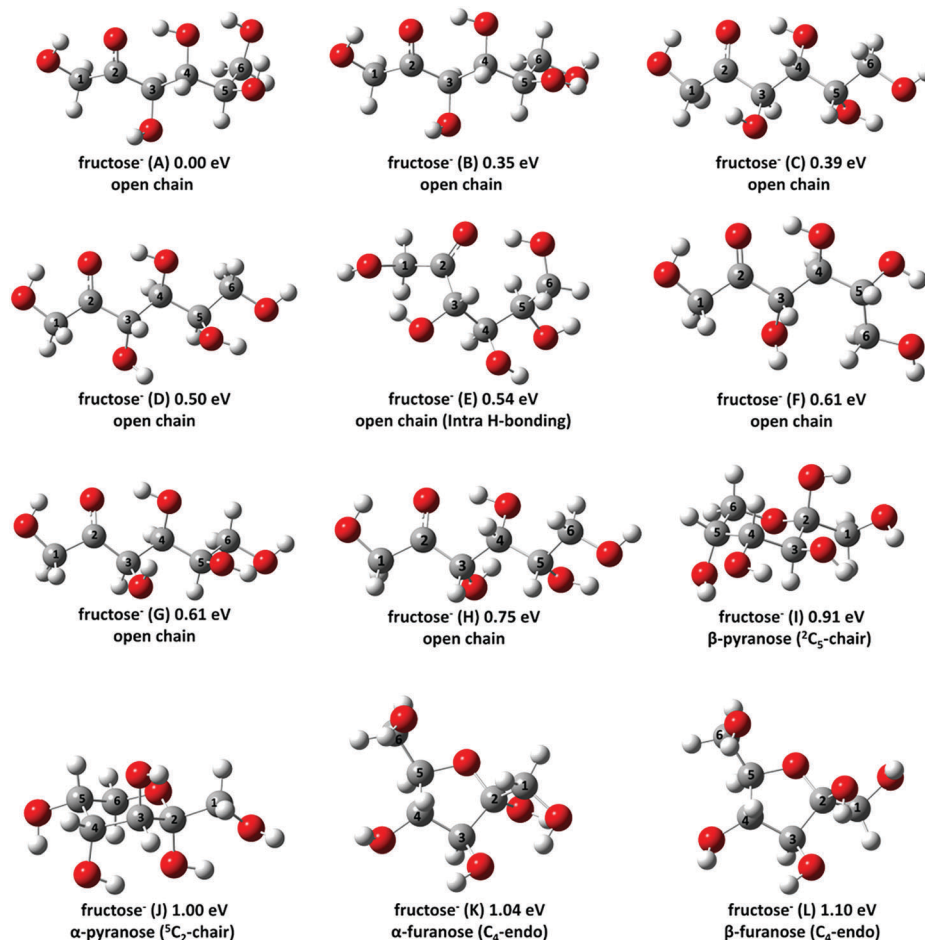
Fig. 7 Optimized geometries of the typical low lying anionic isomers of fructose$^-$ based on B3LYP/6-311++G(d,p) calculations. The relative energies and structural polymorphs[41] are indicated. The C atom numberings are given. For open chain structures (1)C to (6)C is ordered from left to right. For both furanose and pyranose structures (1)C to (6)C is ordered from the right to the left in a clockwise direction. C atom numbering for open chain structures correspond to those in the cyclic structures, for instance (1)C ⇔ (1)C.

contributed by some higher energy isomers with loss of hydrogen from C atoms, see Fig. S8 (ESI†). The (fructose-H) neutral evidences pyranose cyclic and open chain structures as the lowest lying isomers, through loss of (3)H and (4)H, respectively, as shown in Fig. S18 (ESI†). The lowest energy neutral furanose isomer (i) loses (3)H. The preferred H loss positions for neutrals are different from those of anions for open chain, pyranose, and furanose structures.

(Fructose-OH)$^-$ can be optimized from either the parent anion or (fructose-H)$^-$ through loss of an OH group or an O atom, respectively. Fig. 9 displays the low lying isomers of (fructose-OH)$^-$, in which the blue labels indicate structures optimized from the parent anion with loss of one OH group and black labels indicate structures optimized from (fructose-H)$^-$ with loss of one O atom. The most stable isomer (fructose-OH)$^-$ (A) is optimized from parent fructose$^-$ (A) with loss of (3)OH: it has a calculated VDE of 3.23 eV, consistent with the experimental observation ($\sim$2.62 eV to $\sim$4.35 eV) of the broad PES feature. The isomer (fructose-OH)$^-$ (C) also loses (3)OH, but it is optimized from (fructose-H)$^-$ (E) [same as, fructose$^-$ (A) – (3)H] with loss of an O atom. Its relative energy is 0.11 eV and

its calculated VDE is 3.28 eV, in agreement with the experimental feature. The isomer (fructose-OH)$^-$ (B) is developed from (fructose-H)$^-$ (A) [same as, fructose$^-$ (C) – (3)H] followed by loss of an O atom, equivalent to loss of (3)OH. The theoretical VDE for this isomer is calculated to be 3.45 eV, in accordance with the experimental results. The isomer (fructose-OH)$^-$ (J), optimized from the parent fructose$^-$ (C) with loss of (3)OH, has a different structure and a higher relative energy (0.50 eV) compared to isomer (B). These latter two isomers are conformationally different but have the same OH loss position. Other lower lying isomers of (fructose-OH)$^-$ are all open chain structures and also have calculated VDEs in accordance with experimental observations. For high lying furanose and pyranose (fructose-OH)$^-$ isomers, two optimized final structures are similar: isomers (fructose-OH)$^-$ (M) and (O) have the same relative energies and calculated VDEs as those of isomers (N) and (P), respectively, see Fig. 9 and Table 1. Their calculated VDEs are smaller than those of open chain isomers and their relative energies are above 1.24 eV. Clearly, many isomers coexist in the experiments and contribute to the broad feature in the photoelectron spectrum of (fructose-OH)$^-$;
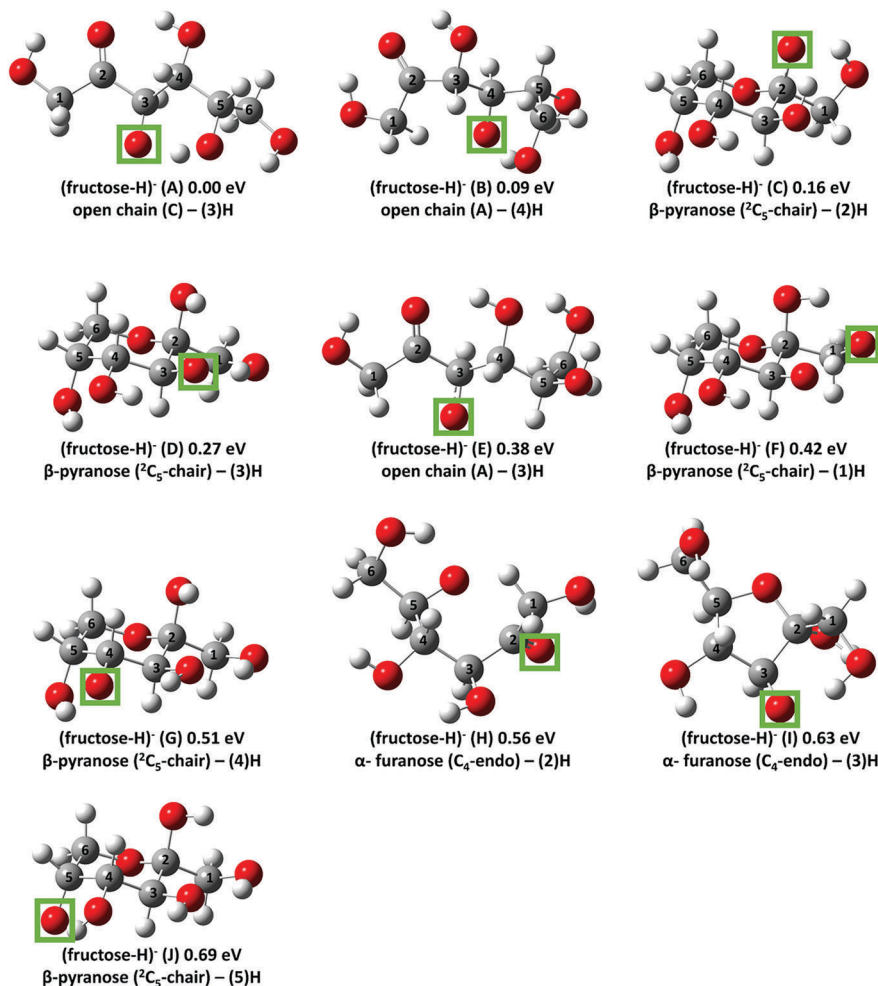
23332 | Phys. Chem. Chem. Phys., 2017, 19, 23325–23344

This journal is © the Owner Societies 2017

Fig. 8 Optimized geometries of the typical low lying anionic isomers of (fructose-H)⁻ based on B3LYP/6-311++G(d,p) calculations. The relative energies and structural polymorphs[41] are indicated. The green square indicates loss of hydrogen at the indicated position. The C atom numberings are given. For open chain structures (1)C to (6)C is ordered from left to right. For both furanose and pyranose structures (1)C to (6)C is ordered from right to left in a clockwise direction. C atom numbering for open chain structures correspond to those in the cyclic structures, for instance (1)C ⇔ (1)C.

however, the main intensity of this PES feature is derived from open chain structures.

The lowest energy isomer of (fructose-OH) neutrals is, consistent with the results for anions and neutrals of the other fructose related species discussed above, not necessarily the lowest energy isomer of (fructose-OH)⁻ anions. Isomer (a) of the (fructose-OH) neutral loses (6)OH from the fructose neutral parent (see Fig. S19 for neutral structures, ESI†). Isomer (b) has a relative energy of 0.33 eV and undergoes a C–C bond breaking, as the HOMO (SOMO) becomes antibonding: both canonical and NBO orbitals generate these electronic and geometric structures. Isomer (c) has a similar geometry to that of anionic isomer (A) and its relative energy is 0.43 eV with respect to the ground state of the neutral. Isomers (h) and (i) have similar structures to those of anionic isomers (B) and (F), respectively. Other lower lying neutrals are also open chain structures, similar to the situation found for anions. Nonetheless, these neutral species must be calculated in order to make this point and additionally to demonstrate that the

anions of (fructose-OH) do not mechanistically directly develop from the neutral species in a simple fashion. More will be presented on these points in the Discussion section below.

Fig. 10 shows the low lying isomers of (fructose-H₂O)⁻. Purple labels in this figure indicate structures optimized from (fructose-OH)⁻ with loss of one H atom and black labels indicate structures optimized from (fructose-H)⁻ with loss of an OH group. Several similar isomers can also be optimized from the fructose⁻ anion with loss of an H₂O group directly, as shown in Fig. S10 (ESI†). The lowest energy isomer (fructose-H₂O)⁻ (A) is optimized from the furanose ring opening isomer (fructose-OH)⁻ (M) with loss of (3)H, generating loss of (6)OH and (3)H: the (2)C–(3)C bond is broken, as above for the (fructose-OH) neutral isomer (b), and two intramolecular H-bonds are formed: again, the canonical and NBO orbitals reflect these changes, as they do for the (fructose-OH) neutral isomer (b). The calculated VDE of isomer (A) is 1.96 eV, in good agreement with the experimental VDE (∼2.13 eV) at the higher EBE component of the PES feature. The C–C bond breaking
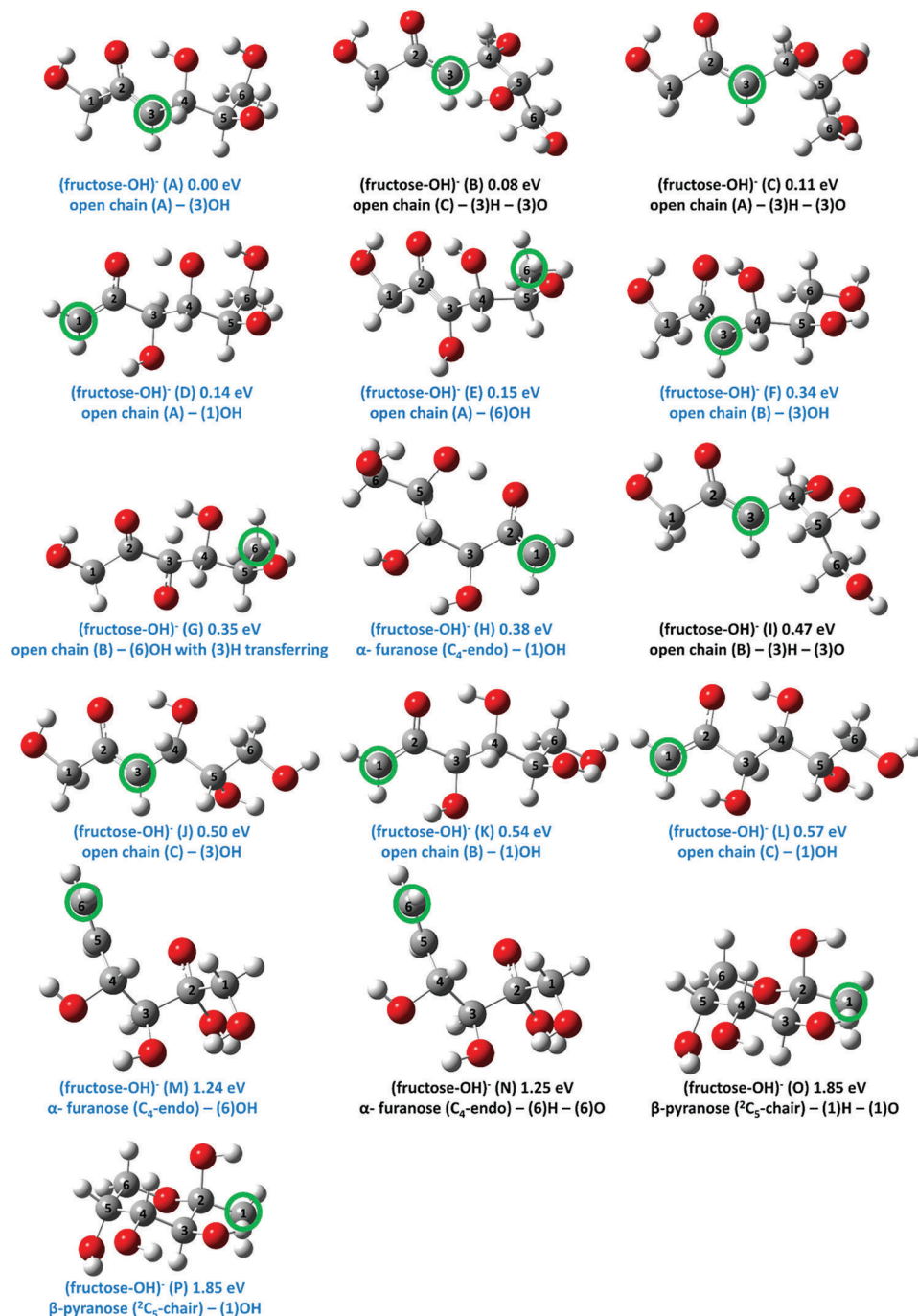
This journal is © the Owner Societies 2017

Phys. Chem. Chem. Phys., 2017, **19**, 23325–23344 | 23333

Fig. 9 Optimized geometries of the typical low lying anionic isomers of (fructose-OH)$^-$ based on B3LYP/6-311++G(d,p) calculations. The relative energies and structural polymorphs[41] are indicated. The green circle indicates loss of an OH group at the marked position. Blue labels indicate structures optimized from the parent anion with loss of one OH group and black labels indicate structures optimized from (fructose-H)$^-$ with loss of one O atom. The C atom numberings are given. For open chain structures (1)C to (6)C is ordered from left to right. For both furanose and pyranose structures (1)C to (6)C is ordered from right to left in a clockwise direction. C atom numbering for open chain structures correspond to those in the cyclic structures, for instance (1)C ⇔ (1)C.

nature will be considered below in the Discussion section. Isomer (fructose-H$_2$O)$^-$ (B) is nearly degenerate in energy with (fructose-H$_2$O)$^-$ isomer (A): it is also optimized from the furanose ring opening isomer (fructose-OH)$^-$ (M) resulting in loss of (6)OH and (3)H. Concurrently, the (2)C–(3)C bond breaks, with one intramolecular H-bond formation. Its calculated

VDE (1.95 eV) also coincides with the higher experimental VDE value of ~2.13 eV. Isomer (fructose-H$_2$O)$^-$ (C) has a relative energy of 0.33 eV, and is optimized from open chain isomer (fructose-OH)$^-$ (B), generating a structure with loss of (3)OH and (5)H: the (4)C–(5)C bond is thereby broken. Isomer (fructose-H$_2$O)$^-$ (D) is degenerate in energy with the isomer
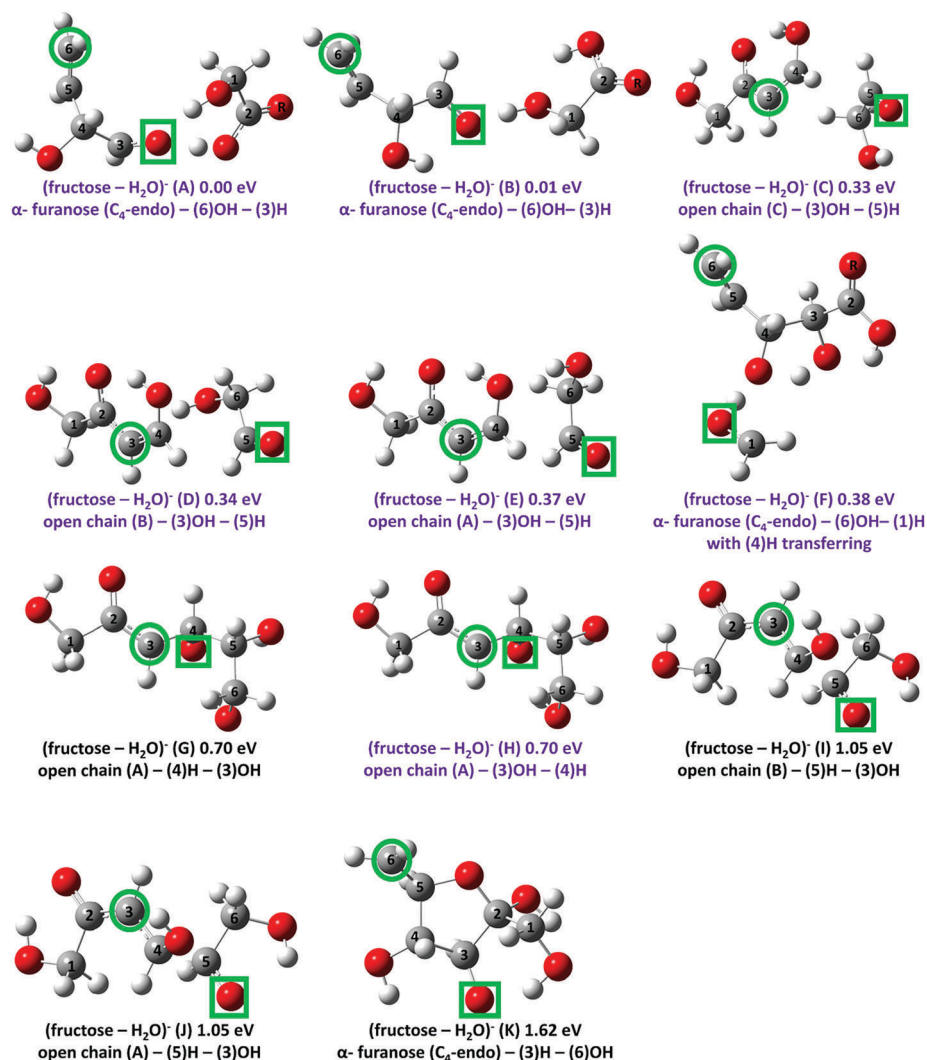
Fig. 10 Optimized geometries of the typical low lying anionic isomers of (fructose-H$_2$O)$^-$ based on B3LYP/6-311++G(d,p) calculations. The relative energies and structural polymorphs[41] are indicated. The green square indicates loss of hydrogen and the green circle indicates loss of an OH group at the marked positions. Purple labels indicate structures optimized from (fructose-OH)$^-$ with loss of one H atom and black labels indicate structures optimized from (fructose-H)$^-$ with loss of an OH group. The C atom numberings are given. For open chain structures (1)C to (6)C is ordered from left to right. For both furanose and pyranose structures (1)C to (6)C is ordered from right to left in a clockwise direction. C atom numbering for open chain structures correspond to those in the cyclic structures, for instance (1)C ⇔ (1)C.

(fructose-H$_2$O)$^-$ (C), optimized from the open chain isomer (fructose-OH)$^-$ (F) also resulting in loss of (3)OH and (5)H, and a broken (4)C–(5)C bond. Similarly, isomer (fructose-H$_2$O)$^-$ (E), optimized from the open chain isomer (fructose-OH)$^-$ (A), yields a geometry for (fructose-H$_2$O)$^-$ with loss of (3)OH and (5)H, and incurs (4)C–(5)C bond breaking: both canonical and NBO orbitals show anti-binding electronic distributions between these C atoms. Isomers (fructose-H$_2$O)$^-$ (C), (D), and (E) are of conformational nature. Their calculated VDEs are 1.48 eV, 1.54 eV, and 1.57 eV, respectively, consistent with the experimental VDE (~1.55 eV) of the lower EBE part of the PES feature. The isomer (fructose-H$_2$O)$^-$ (F) is optimized from the furanose ring opening isomer (fructose-OH)$^-$ (M) with loss of (1)H and (1)C–(2)C bond breaking. Its calculated VDE is 3.39 eV, larger than the experimental value. All other optimized structures of

(fructose-H$_2$O)$^-$ without C–C bond breaking have higher relative energies (above 0.70 eV) with respect to the lowest energy isomer and larger VDEs than the experimentally observed ones. Therefore, the higher EBE component of the (fructose-H$_2$O)$^-$ PES feature is generated by contributions from isomers (fructose-H$_2$O)$^-$ (A) and (B), while the lower EBE part is generated by contributions from (fructose-H$_2$O)$^-$ (C), (D), and (E). Isomer (F) may contribute to the tail of the PES feature. The different PES feature components (intensity peaks) are generated by different positional isomers; the same PES feature components are composed of contributions from different conformational isomers. The most stable neutral isomer (fructose-H$_2$O) (a) does not incur C–C bond breaking and has an open chain structure with loss of (5)H and (6)OH, evidencing H transferring from (5)C to (6)C (see Fig. S20, ESI†).

Note that for many of these isomeric forms the basic anionic or neutral structure need not have the same consistent open chain or ring structures. Thereby, the VDEs will arise from a consistent geometrical structure, that of the anion, while the EAs (electron affinities) must be calculated at both open chain and ring structures.

VI. Discussion

(A). Anionic species

Fructose⁻. Based on the good agreement between the PES data and the B3LYP calculations, open chain fructose⁻ structures are determined to exist in the gas phase. These and other isomers of the fructose⁻ anion are generated through the MALDI method: the lower energy fructose⁻ isomers are the open chain ones. Pyranose and furanose anionic conformations are absent in the gas phase presumably because of their very low electron binding energies ($\sim$ 0.10 eV), as well as their higher energies compared to open chain structures. Loss of one H atom, an OH group, or one H_2O moiety is characteristic of anionic fragmentation under the present experimental conditions.

(Fructose-H)⁻. (Fructose-H)⁻ evidences both open chain and pyranose structures through loss of an H atom at different positions. The lowest energy open chain structure loses (3)H and the lowest energy pyranose structure loses (2)H.

(Fructose-OH)⁻. (Fructose-OH)⁻ primarily exists as an open chain isomeric structure, mainly of positional nature at (3), (6), and (1): additional conformational differences for each positional isomer are also present. These conformational and positional open chain isomers coexist in the beam and contribute to the broad feature in the photoelectron spectrum of (fructose-OH)⁻. The open chain (fructose-OH)⁻ species have lower energy than cyclic conformations. Thus, (fructose-OH)⁻ mainly exists as an open chain structure in the experiments, different from the situation of (fructose-H)⁻, which has both open chain and pyranose structures present in the gas phase. The unfavorable cyclic structures of (fructose-OH)⁻ compared to the situation for (fructose-H)⁻ may be rationalized by the fact that the number of intramolecular H-bonds decreases with loss of an OH group. This loss of hydrogen bonding destabilizes cyclic conformations.

(Fructose-H₂O)⁻. (Fructose-H₂O)⁻ has two types of positional isomers, each contributing separately to the higher and lower EBE components of the broad PES feature. One of these positional isomers undergoes loss of (6)OH and (3)H, and the other undergoes loss of (3)OH and (5)H. The (6)OH/(3)H isomer starts from a furanose ring structure and the (3)OH/(5)H isomer originates from an open chain structure. They both show C–C bond breaking: the (6)OH/(3)H isomer undergoes hydrogen bond formation, which helps to stabilize these structural species.

As briefly described in the Introduction section, upon capture of a low energy electron, both ribose and deoxyribose can undergo loss of one or two water molecules, as occurs for fructose. The (fructose-H₂O)⁻ anion can be generated as a direct decomposition product from the parent fructose neutral

upon attaching an extra electron, as will be demonstrated below by calculation of the thermodynamics of anion generation mechanisms. The (fructose-H₂O)⁻ (6)OH/(3)H isomers originate from a parent furanose cyclic structure, which undergoes decomposition reactions leading to the degradation of the cyclic structure (ring opening) and loss of water. The (6)OH/(3)H isomers behavior can be compared to the sugar moiety behavior of DNA/RNA, because both deoxyribose and ribose present a furanose cyclic structure in these biopolymer backbone supports.

Experimental and theoretical studies of ribose related monosaccharides are currently underway in our laboratory, and their results can be compared with those for fructose reported herein. So far, (fructose-H₂O)⁻ and (ribose-H₂O)⁻ show similar photoelectron spectral features but with different assigned structures: (ribose-H₂O)⁻ prefers isomers derived only from open chain structures with loss of H from C atoms. Isomers of (ribose-H₂O)⁻ derived from furanose cyclic structures, have higher relative energies than the lowest energy isomer of (ribose-H₂O)⁻. The calculated VDEs of these isomers also do not agree with the experimental VDEs. Recall that (fructose-H₂O)⁻ can derive from both open chain and furanose structures. This shows that ribofuranose has a lower decomposition probability upon attaching an extra electron through loss of water compared to fructofuranose. Therefore, one can tentatively conclude that ribofuranose is more stable than fructofuranose. This could be one reason why ribose is chosen for the RNA backbone but not fructose, since the sugar moiety presents a furanose cyclic structure in DNA/RNA backbone supports. The exclusively selected ribose/deoxyribose in nucleic acids may not be completely addressed by the above conclusions. Other factors may include, for instance, (1) chemical stability, (2) rigidity of nucleotides, (3) sugar puckering, (4) maintenance of steric freedom, and (5) reduction of nonbonded interactions.[75]

The C–C bond breaking occurring for the assigned anionic isomers of (fructose-H₂O)⁻ can be understood through examination of electron distribution maps based on an NBO (and canonical orbital) analysis, as well as through changes in the C–C bond length (see Fig. S29, S30 and Table S2, ESI†). The (6)OH/(3)H isomer shows no bond suggestion between (2)C and (3)C: the distance between (2)C and (3)C atoms increases from 1.55 Å for the parent anionic isomer to $\sim$4.27 Å for the stable optimized (fructose-H₂O)⁻ species. Similarly, the (fructose-H₂O)⁻ (3)OH/(5)H isomer, as shown in Fig. S30 and Table S2 (ESI†), evidences no obvious bonding character between (4)C and (5)C: the (4)C and (5)C separation lengthens from $\sim$1.5 to 2.89 Å following optimization of this isomer. These isomers are still bound as a single unit even after passing through the extraction, field free TOFMS flight tube, and reflectron regions: they are stable on the experimental timescale (hundreds of microseconds), and are finally observed as bound single mass unit species in our mass spectra. These structures are thought to be correct because of the accurately calculated VDEs of all the isomers of fructose related anions and their associated structures, which are apparently reasonable based on previous reported work.[64]

23336 | *Phys. Chem. Chem. Phys.,* 2017, **19**, 23325–23344

This journal is © the Owner Societies 2017

Other positional and conformational isomers of (fructose-H_2O)$^-$ without C–C bond breaking have higher energies than the observed ones, in contrast to the neutral species for which C–C bond retention yields the most stable structure (see Fig. 10 and Fig. S20 (ESI†). The presence of an extra electron increases the energy released during the dehydration process. (Fructose-H_2O)$^-$ fragments with different EBEs have specific loss positions for OH and H. Note that this circumstance is different from that observed for the positional isomers of (fructose-H)$^-$ and (fructose-OH)$^-$, which have similar EBEs (see Fig. 8 and 9). Thus, dehydration positions are uniquely assigned for the (fructose-H_2O)$^-$ anion, in contrast to the dissociation sites for H or OH separately.

The C–C bond breaking character is unique for anionic (fructose-H_2O)$^-$ among the four fructose related anionic species, further demonstrating the active nature of fructose upon capturing an extra electron.

(B) Anion and neutral species generation mechanisms

Employing the MALDI method for generation of the four, fructose related anionic species discussed above, observed relative and absolute concentrations of each anion depend on the sample desorption substrate. The particular isomer observed for the parent anion fructose$^-$ is also desorption metal substrate dependent (see Fig. 4). This observation suggests that surface chemistry participates in the generation process of fructose related anions. As shown in Table 2, different properties of the substrates are explored and compared, including electron affinity of the metal atom, work function of the solid, and surface structure, composition, and chemistry. A Zn substrate has the lowest work function and a negative electron affinity; as such, Zn may produce more electrons during the MALDI/ablation process and thereby generate more fructose related anion species. Parent anion conformation is also substrate dependent: the conformational ratio of fructose in liquid has been reported to be solvent dependent as well.[76–79]

The identification of only an open chain fructose$^-$ parent anion in the gas phase suggests two possible generation pathways for these parent anions. First, the open chain fructose anion can come from ring opening of the neutral pyranose structure through the MALDI process. The calculated reaction ΔH (−EA + cyclic to open chain reaction, −19 kcal mol^{-1}) from the neutral β-pyranose fructose to the anionic open chain isomer (A) further supports this

ring opening process. Although the β-pyranose structure has an electron affinity near zero (~ 0.06 eV), the ring opening from the β-pyranose neutral to the open chain anion can occur through the MALDI process. Second, another reaction channel can be based on an open chain neutral fructose molecule attaching an extra electron, since calculations show that the open chain structure and pyranose structure have comparable energy. The enthalpy change for this reaction is −EA $\sim$ −1 eV or $\sim$ −22 kcal mol^{-1} [(A) isomer]. Thus, reaction from the fructose neutral to the fructose anion is thermodynamically allowed through both the above channels. This observation of open chain conformations is consistent with previous spectroscopic evidence that abundant open chain conformations of anionic aldohexoses exist in the gas phase.[38]

The observed fructose related anion fragment (fructose-X)$^-$ species can be generated through three general mechanisms: (1) MALDI/ablation/surface related processes such that every species is present in the beam following laser ablation; (2) stepwise evolution of isolated anion species before product anions leave the extraction region; and (3) stepwise evolution of isolated neutral species which attach an electron before product anions leave the extraction region. The first option for a mechanism can only be suggested if the second and third options are eliminated based on consideration of the overall reaction enthalpy and entropy for all possible specific pathways. The possible pathways for stepwise generation of various fructose related anionic fragment species are outlined in Fig. 11. ΔH values for different possible reaction pathways for generating specific fructose related anionic, isomeric species are summarized in Fig. 12. For calculation of ΔH values for the generation of specific fragment isomers, the reactant that has structures similar to that of the final product is chosen. What follows is the detailed analysis of these results and conclusions where possible.

Possible anionic mechanisms (reaction pathways) for the formation of various observed fructose$^-$ related anionic fragment species. As shown in Fig. 11, red colored reaction equations indicate possible anionic reaction pathways. For (fructose-H)$^-$, open chain structures can develop from the parent open chain anion by loss of one H atom. The formation pathway for cyclic structures of (fructose-H)$^-$ from cyclic parent anion structures is energetically unfavorable because cyclic parent anions have considerably higher relative energies with respect to open chain ones and are therefore less populated. In order to verify if this

Table 2 Electron affinities of metal atoms, work functions of solid surfaces, surface quality of different substrates, and the minimal ablation laser energy for producing fructose related anion species

	Filter paper	Cu	Ti	Al	Zn	Au
Electron affinity of metal (eV)	—	1.235	0.079	0.433	Negative	2.31
Work function (φ/eV)	—	4.65	4.10	4.28	3.63	5.10
Surface quality	—	Less oxidation	Oxidized on exposure to air	Al_2O_3 forms on exposure to air	Strong reducing agent, form $Zn_5(OH)_6(CO_3)_2$, by reaction with atmospheric CO_2	Least oxidation
Minimal ablation laser energy (mJ per pulse)	7–9	$\sim$5	$\sim$5	$\sim$6	$\sim$2.5	$\sim$13

This journal is © the Owner Societies 2017

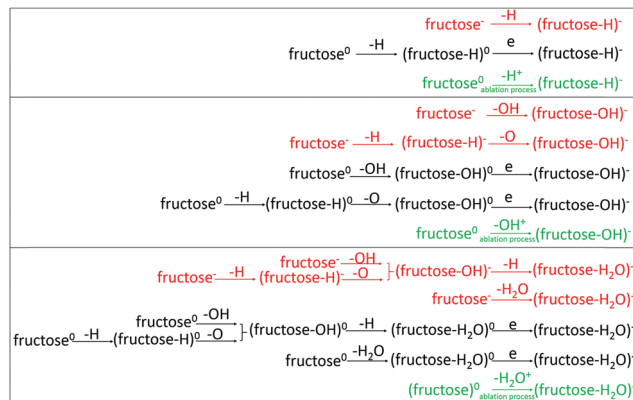*Phys. Chem. Chem. Phys.*, 2017, **19**, 23325–23344 | **23337**

Fig. 11 The different possible reaction pathways for generating various fructose related anionic species. Red color indicates an anionic mechanism. Black color indicates a neutral mechanism. Green color indicates a possible mechanism during the laser ablation process.

reaction can occur, each anionic reaction pathway ΔH is calculated for isomers (fructose-H)$^-$ (A), (B), and (C): all of the calculated enthalpy changes are positive, implying that these reactions are thermodynamically forbidden (Fig. 12). By considering the reaction ΔGs, a temperature of >1000 K is required for product formation. Since this high temperature is unlikely following beam supersonic expansion, this reaction mechanism is unlikely for generating isolated (fructose-H)$^-$ from isolated fructose$^-$.

(Fructose-OH)$^-$ open chain structures can arise from either open chain structures of (fructose-H)$^-$ through loss of an O atom or through open chain fructose$^-$ structures through loss of an OH group. The geometry optimized from the parent anion through loss of an OH group is different from that coming from (fructose-H)$^-$ followed by loss of O. The positive ΔHs for anionic reaction pathways for generating isomers (fructose-OH)$^-$ (A), (B), and (C) demonstrate that they too are thermodynamically inaccessible (see Fig. 12(a)). By considering reaction ΔGs, a temperature of >3000 K is required for these pathways to be active.

For (fructose-H$_2$O)$^-$, the lower EBE isomers come from open chain structures (fructose-(3)OH)$^-$ through loss of an H atom, see Fig. 10. They are optimized from three open chain lower lying isomers of (fructose-(3)OH)$^-$ through loss of an H atom: the (4)C–(5)C bond of these conformers is broken, resulting in loss of (5)H. All other optimized structures of (fructose-H$_2$O)$^-$ from other open chain (fructose-OH)$^-$ with loss of H or from (fructose-H)$^-$ with loss of OH, without C–C bond cleavage, have higher relative energy (>0.38 eV) with respect to the lowest energy isomer of (fructose-H$_2$O)$^-$ and larger VDEs than the experimentally observed ones. The reaction pathway for the formation of the higher EBE isomers of (fructose-H$_2$O)$^-$ from (fructose-OH)$^-$ is energetically less favorable. The higher EBE isomers that do contribute to the observed PES feature for (fructose-H$_2$O)$^-$ are optimized from high lying furanose ring opening species of (fructose-OH)$^-$ by losing one H atom, with (2)C–(3)C bond breaking and intramolecular H-bond formation, generating a product with loss of the (6)OH group

and the (3)H atom. The furanose ring opening structure of (fructose-OH)$^-$ employed for generating the higher observed EBE isomers of (fructose-H$_2$O)$^-$ has relative energy of 1.24 eV with respect to the ground state isomer of (fructose-OH)$^-$ and is less populated. Among the different anionic reaction pathways, ΔHs of reactions from both (fructose-OH)$^-$ and (fructose-H)$^-$ to (fructose-H$_2$O)$^-$ are all positive (see Fig. 12(b)). Nonetheless, ΔHs from parent anions with loss of one H$_2$O give rise to negative values of the reaction enthalpy change. Results of these calculations suggest that anionic reaction pathways for generating both higher and lower EBE isomers of (fructose-H$_2$O)$^-$ through direct loss of an H$_2$O molecule from parent anions is thermodynamically allowed. Other anionic pathways for this species are thermodynamically forbidden.

Possible neutral reactant mechanisms (reaction pathways) for the formation of various observed fructose related anionic fragment species. As shown in Fig. 11, the black color indicates the possible neutral reactant pathways for the different fructose related anion fragments. For (fructose-H)$^-$, both open chain and cyclic conformations come from the parent neutral through loss of an H atom followed by attachment of an extra electron: the lowest energy neutral fructose isomers include both open chain and pyranose structures that are nearly degenerate in energy. (Fructose-H)^0 also evidences open chain and pyranose ring structures nearly degenerate in energy as its lowest energy isomers. Such a mechanism can also be considered as a deprotonation process: the proton/H atom loss position from the parent neutral to form (fructose-H)$^-$ can show the individual acidities for the different hydroxyl groups. The anomeric hydroxyl group (2) can consequently be considered the most acidic one for the pyranose structure, consistent with previous theoretical reports.[24] The positive ΔHs for neutral reaction pathways reveal that they are thermodynamically forbidden, for reasonable temperatures (see Fig. 12(a)).

The major portion of the (fructose-OH)$^-$ open chain structures are less likely to arise from (fructose-OH)^0 followed by electron attachment because the (fructose-OH)^0 isomers with structures similar to those lower lying anionic isomers have a relative energy above 0.43 eV with regard to the lowest energy isomer of (fructose-OH)^0, see Fig. S19 (ESI†). They are therefore probably less populated in the gas phase beam sample. The positive ΔH results further support forbidden neutral reaction pathways for this anion.

(Fructose-H$_2$O)$^-$ may be generated by a parent neutral losing one H$_2$O molecule followed by attachment of an extra electron. Several low lying isomers of neutral (fructose-H$_2$O)^0 can generate the observed (fructose-H$_2$O)$^-$. These species all undergo C–C bond rupture. (Fructose-H$_2$O)^0 can also be generated from (fructose-OH)^0 through loss of one H atom or from (fructose-H)^0 through loss of an OH group. The (fructose-OH)^0 isomers for generating (fructose-H$_2$O)^0 followed by attachment of an extra electron to form (fructose-H$_2$O)$^-$ with the observed PES VDE feature have a relative energy of 0.43 eV with respect to the most stable isomer of (fructose-OH)^0. These higher energy isomers of (fructose-OH)^0 should be less populated than the lower energy ones in the supersonically expanded beam.

23338 | *Phys. Chem. Chem. Phys.*, 2017, **19**, 23325–23344

This journal is © the Owner Societies 2017

(a)

(fructose-H)⁻

fructose⁻ ⟶ (fructose-H)⁻ + H

Isomers of (fructose-H)⁻	ΔH without BSSE (kcal/mol)	ΔH with BSSE (kcal/mol)	BSSE (kcal/mol)
(A) open chain	27.26	27.04	0.21
(B) open chain	38.87	38.27	0.60
(C) pyranose	19.41	19.11	0.30

fructose⁰ ⟶ (fructose-H)⁰ + H —e→ (fructose-H)⁻ + H

Isomers of (fructose-H)⁻	ΔH without BSSE (kcal/mol)	ΔH with BSSE (kcal/mol)	BSSE (kcal/mol)
(A) open chain	12.45	12.14	0.31
(B) open chain	16.68	16.27	0.41
(C) pyranose	20.91	20.55	0.36

(fructose-OH)⁻

fructose⁻ ⟶ (fructose-OH)⁻ + OH fructose⁻ ⟶ (fructose-H)⁻ + H ⟶ (fructose-OH)⁻ + O + H		(fructose-H)⁻ ⟶ (fructose-OH)⁻ + O	
Isomers of (fructose-OH)⁻	ΔH (kcal/mol)	Isomers of (fructose-OH)⁻	ΔH (kcal/mol)
(A)	30.75 / 196.54	(A)	150.81
(B)	23.52 / 189.32	(B)	162.05
(C)	33.69 / 199.48	(C)	153.75

fructose⁰ ⟶ (fructose-OH)⁰ + OH —e→ (fructose-OH)⁻ + OH
fructose⁰ ⟶ (fructose-H)⁰ + H ⟶ (fructose-OH)⁰ + O + H —e→ (fructose-OH)⁻ + O + H

Isomers of (fructose-OH)⁻	ΔH (kcal/mol)
(A)	8.55 / 174.35
(B)	8.71 / 174.51
(C)	11.49 / 177.29

(fructose-H)⁰ ⟶ (fructose-OH)⁰ + O —e→ (fructose-OH)⁻ + O

Isomers of (fructose-OH)⁻	ΔH (kcal/mol)
(A)	77.35
(B)	79.66
(C)	80.29

(b)

(fructose-H₂O)⁻

fructose⁻ ⟶ (fructose-OH)⁻ + OH ⟶ (fructose-H₂O)⁻ + H + OH
fructose⁻ ⟶ (fructose-H)⁻ + H ⟶ (fructose-OH)⁻ + O + H ⟶ (fructose-H₂O)⁻ + H + O + H
fructose⁻ ⟶ (fructose-H₂O)⁻ + H₂O

Isomers of (fructose-H₂O)⁻	ΔH (kcal/mol)
(A)	78.13 / 243.93 / -36.64
(C)	100.05 / 265.85 / -14.72

fructose⁰ ⟶ (fructose-OH)⁰ + OH ⟶ (fructose-H₂O)⁰ + H + OH —e→ (fructose-H₂O)⁻ + H + OH
fructose⁰ ⟶ (fructose-H)⁰ + H ⟶ (fructose-OH)⁰ + O + H ⟶ (fructose-H₂O)⁰ + H + O + H —e→ (fructose-OH)⁻ + H + O + H
fructose⁰ ⟶ (fructose-H₂O)⁰ + H₂O —e→ (fructose-H₂O)⁻ + H₂O

Isomers of (fructose-H₂O)⁻	ΔH (kcal/mol)
(A)	80.13 / 245.92 / -34.65
(C)	85.25 / 251.04 / -29.53

(fructose-OH)⁻ ⟶ (fructose-H₂O)⁻ + H		(fructose-H)⁻ ⟶ (fructose-H₂O)⁻ + OH	
Isomers of (fructose-H₂O)⁻	ΔH (kcal/mol)	Isomers of (fructose-H₂O)⁻	ΔH (kcal/mol)
(A)	76.53	(A)	46.22
(C)	42.14	(C)	72.79

(fructose-OH)⁰ ⟶ (fructose-H₂O)⁰ + H —e→ (fructose-H₂O)⁻ + H		(fructose-H)⁰ ⟶ (fructose-H₂O)⁰ + OH —e→ (fructose-H₂O)⁻ + OH	
Isomers of (fructose-H₂O)⁻	ΔH (kcal/mol)	Isomers of (fructose-H₂O)⁻	ΔH (kcal/mol)
(A)	-17.55	(A)	-20.05
(C)	9.53	(C)	-9.61

Fig. 12 (a) Calculated ΔH values for different possible reaction pathways for generating specific fructose related anionic species isomers. Red color indicates an anionic mechanism. Black color indicates a neutral mechanism. The ΔH values for (fructose-H)⁻ include ΔH with/without BSSE and the BSSE is also provided. All calculated ΔH values for both (fructose-OH)⁻ and (fructose-H₂O)⁻ are ΔH without BSSE. For calculating the ΔH values of a specific isomer, the reactant that has a similar structure to that of the final product is chosen. ΔH for the neutral reactant species adding an electron to generate the related anion is −EA of the reactant (see ref. 47). (b) Calculated ΔH values for different possible reaction pathways for generating specific fructose related anionic species isomers. Red color indicates an anionic mechanism. Black color indicates a neutral mechanism. The ΔH values for (fructose-H)⁻, (fructose-OH)⁻, and (fructose-H₂O)⁻ are provided without BSSE correction. For calculating ΔH values of a specific isomer, the reactant that has a similar structure to that of the final product is chosen. ΔH for the neutral reactant species adding an electron to generate the related anion is −EA of the reactant (see ref. 47).

Reaction pathways from such higher energy (fructose-OH)^0 isomers to (fructose-H$_2$O)^0 isomers may therefore not contribute significantly to the total (fructose-H$_2$O)$^-$ signal intensity. As shown in Fig. 12(b) by the calculated negative ΔH values, neutral reaction pathways for generating higher and lower EBE isomers arising from the parent neutral by losing one H$_2$O molecule directly are thermodynamically allowed. Both higher and lower EBE isomers can also develop from (fructose-OH)^0 or (fructose-H)^0 based on reaction thermodynamics. The (fructose-H)^0 reaction channel optimization generates (fructose-H$_2$O)$^-$ anions with VDEs outside the experimentally observed PES values (for instance, isomers (fructose-H$_2$O)$^-$ (I) and (J) in Fig. 10).

This demonstrates that from the thermodynamic point of view, loss of a water molecule from neutral fructose is exothermic; however, this dehydration must be kinetically unfavorable, due to a large activation barrier, because fructose exists as a stable compound on a macroscopic time scale, even in the gas phase. The availability of an extra electron and the positive electron affinity of (fructose-H$_2$O)^0 energetically drive the reaction. The most stable structure of (fructose-H$_2$O)^0 does not have a broken C–C structure, suggesting that the presence of an extra electron weakens the C–C chemical bonding and leads to dehydration with broken C–C bonds for the (fructose-H$_2$O)$^-$ anion.

In order to determine a particular reaction pathway for the generation of a particular fructose related anion, a potential energy surface with reaction intermediates and transition states must be calculated. These determinations are beyond the scope of the present study. Clearly, (fructose-H)$^-$ and (fructose-OH)$^-$ are more likely initially present in the beam following the MALDI/surface/laser ablation processes, consistent with the experimental observation of substrate dependence of anion concentrations in the beam. Nonetheless, both neutral and ionic mechanisms are contenders for the presence of the observed (fructose-H$_2$O)$^-$ species, and probably both contribute to the finally observed experimental PES feature.

(C) Natural bond orbital (NBO) analysis of the observed fructose related anionic species behavior

For a further electronic structure based understanding the observed fructose related anionic species behavior, a Natural Bond Orbital (NBO) analysis is performed based on B3LYP/6-311++G(d,p) calculations. The molecular orbitals of specific isomers of fructose$^-$, (fructose-H)$^-$, (fructose-OH)$^-$, and (fructose-H$_2$O)$^-$, as well as corresponding neutrals, generated from an NBO analysis, are presented in Fig. 13–16 and Fig. S32–S35 (ESI†).

As shown in Fig. 13, the HOMOs (highest occupied molecular orbitals) of the lowest energy pyranose and the lowest energy furanose structures of fructose$^-$ display diffuse dipole-bound states in which the excess electron is mainly bound around the (1)H and (3)H atoms for the pyranose and the (4)H atom for furanose structures. The dipole moments of pyranose and furanose neutrals are 4.0 D and 2.6 D, respectively, supporting the dipole-bound nature of the respective anions. The HOMO of the lowest energy open chain structure of fructose$^-$ mostly shows p orbital character on (2)C, a valence bound anionic nature. These electronic distributions further demonstrate that
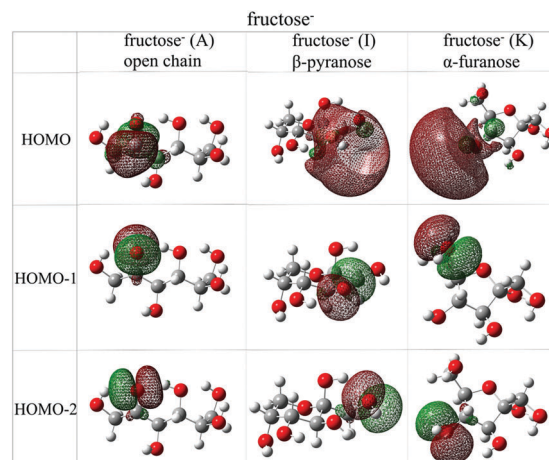

Fig. 13 Molecular orbitals of the lowest energy open chain, pyranose, and furanose structures of the fructose$^-$ anion from an NBO analysis based on B3LYP/6-311++G(d,p) calculations. Only the open chain structure of the fructose$^-$ anion is present in the experiments. The molecular orbitals of the lowest energy pyranose and furanose structures of the fructose$^-$ anion are also provided to compare with the open chain structure.
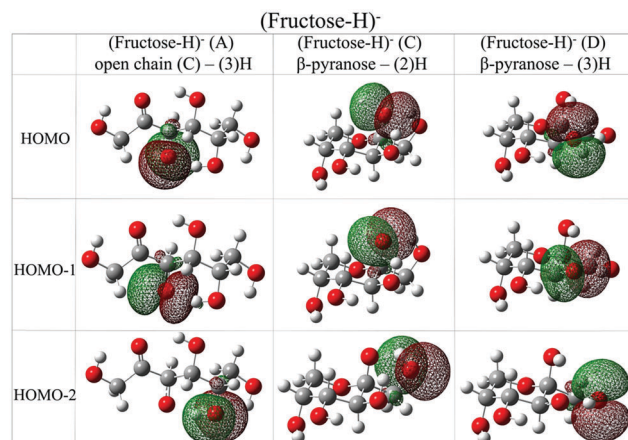

Fig. 14 Molecular orbitals of the lowest energy open chain and two lower lying pyranose structures of the (fructose-H)$^-$ anion from an NBO analysis based on B3LYP/6-311++G(d,p) calculations. They are assigned to be present in the experiment based on the good agreement between experimental and theoretical VDEs.

open chain structures are more stable than cyclic structures for the fructose$^-$ parent anion. This result is consistent with other theoretical investigations, which also find that the fructose$^-$ pyranose anion possesses a dipole-bound state while the open chain isomer evidences a more stable valence bound anion state.[54,80] As shown in Fig. S32 (ESI†), the LUMO (lowest unoccupied molecular orbital) of the open chain structure of neutral fructose is similar to the HOMO of the corresponding anion, while LUMOs of pyranose and furanose structures display a σ^* orbital character of the C–O bond, different from the dipole-bound nature of the HOMO for the corresponding anions.

As shown in Fig. 14, the HOMO and HOMO−1 of open chain and pyranose structures for (fructose-H)$^-$ evidence p orbitals on O atoms upon loss of H atoms. The preference for losing (2)H
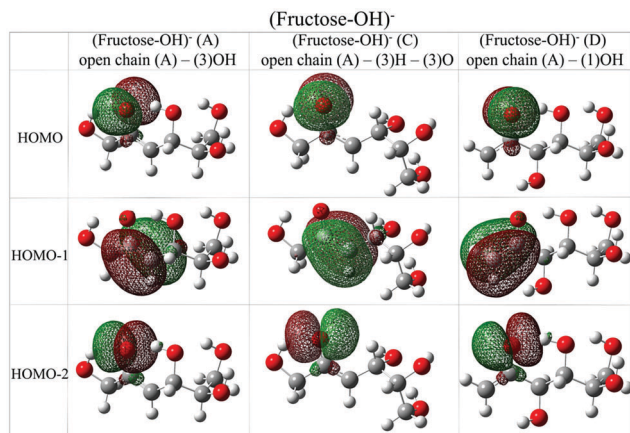
Fig. 15 Molecular orbitals of three open chain isomers (A), (C), and (D) of the (fructose-OH)⁻ anion from an NBO analysis based on B3LYP/6-311++G(d,p) calculations. These three open chain structures are all developed from the parent anion fructose⁻ open chain (A) isomer with compositional and positional differences. They are assigned to be present in the experiments based on the good agreement between experimental and theoretical VDEs. These molecular orbitals of these three isomers are similar.
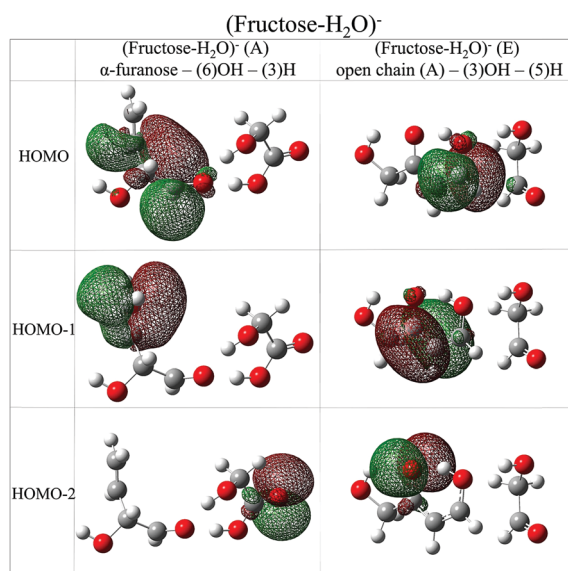

Fig. 16 Molecular orbitals of two positional isomers (A) and (E) of (fructose-H₂O)⁻ anion from an NBO analysis based on B3LYP/6-311++G(d,p) calculations. They are assigned to be present in the experiments, contributing to higher and lower electron binding energy components of the observed PES feature, respectively, based on the good agreement between experimental and theoretical VDEs.

from a pyranose structure, however, is not obvious based on the NBO orbital distributions.

For illustrating the molecular orbitals of (fructose-OH)⁻, three open chain isomers with both conformational and positional nature are displayed in Fig. 15. The HOMOs of the three open chain isomers all show a p orbital character at their (2)O atoms. The (HOMO−1)s of these three open chain isomers are composed of C π orbitals between the C atom with loss of

an OH group ((1) or (3)) and the neighboring adjacent (2)C. The (HOMO−2)s for these species are of a p orbital character at (2)O for all three isomers. The similarity in these high energy occupied molecular orbitals of the three conformational and positional isomers further supports their similar VDEs.

For (fructose-H₂O)⁻, as shown in Fig. 16, the HOMOs of two positional isomers are both mainly comprised of p orbitals of C atoms incurring C–C bond breaking. The site selective nature of the formation mechanism is not readily evident based on the NBO analysis.

VII. Conclusions

(1) Electron binding energy determined and anionic structures assigned based on agreement between experimental and theoretical PES VDE results.

Anion photoelectron spectroscopy, coupled with DFT calculation studies, is applied to all four detected fructose related anion species: fructose⁻, (fructose-H)⁻, (fructose-OH)⁻, and (fructose-H₂O)⁻. Their vertical detachment energies are determined and their anionic and related neutral structures are assigned based on PES and DFT calculations.

For each species, different isomers can be identified as conformational, positional, or both. Conformational isomers have different geometries but the same positions for loss of one H atom or OH group. Positional isomers have different fragmented moiety positions but with similar conformations.

The fructose⁻ parent anion is observed for the first time in the gas phase. It exists as a single, dominant open chain structure, the particular isomer of which is desorption metal substrate dependent, as summarized below. With a Zn substrate, one higher electron binding energy (EBE) open chain isomer and two lower EBE open chain isomers are observed and conformationally characterized, each with different OH group orientations. Only the higher EBE isomer is accessible employing an Al substrate. An NBO analysis for the pyranose and furanose parent anions shows that the HOMOs for these cyclic structures are of a dipole-bound state nature, different from the more stable valence-bound anion nature of the open chain structure.

For the (fructose-H)⁻ anion, many isomers coexist in the gas phase, including open chain and pyranose structures. They are of both conformational and positional nature. The lowest energy open chain isomer loses hydrogen from the oxygen on carbon 3 ((3)H), and the lowest energy pyranose isomer loses hydrogen from the O on carbon 2, (2)H.

Many conformational and positional isomers of (fructose-OH)⁻ also coexist; they are mainly of open chain structures with loss of (3)OH, (1)OH, or 6(OH).

(Fructose-H₂O)⁻ is present in these samples as two kinds of positional isomers, one with loss of the (6)OH group and (3)H from a furanose ring opening structure, and the other with loss of the (3)OH group and (5)H from an open chain structure. The first kind of positional isomer ((6)OH/(3)H) includes two conformational isomers, which contribute to the higher EBE component of the broad PES feature. The second kind of

This journal is © the Owner Societies 2017

Phys. Chem. Chem. Phys., 2017, **19**, 23325–23344 | **23341**

positional isomer ((3)OH/(5)H) has three conformational isomers, which contribute to the lower EBE part of the broad PES feature. Both kinds of positional isomers promote C–C bond breaking: the former isomers ((6)OH/(3)H) involve intramolecular hydrogen bonding and ring opening. (Fructose-H_2O)$^-$ structures further emphasize the energy release process from fructose as an important biomass system.

Based on the good agreement between experimental and theoretical vertical detachment energies, the B3LYP/6-311++G(d,p) level of theory serves as an effective compromise algorithm from the point of view of both computational accuracy and cost for anionic fructose species.

(2) Substrate dependence of anion concentration and conformation speciation is detected.

The MALDI method for the generation of fructose related anion species yields a number of isolated fructose related anions, the concentrations of which depend on different sample desorption substrates. This observation suggests that surface chemistry participates in the generation process of fructose related anions. Five sample desorption substrates, filter paper, Cu, Ti, Al, and Zn, give rise to (fructose-H)$^-$ and (fructose-H_2O)$^-$ anions. A Zn substrate (some surface $Zn_5(OH)_6(CO_3)_2$) generates the highest intensity of (fructose-H)$^-$ and (fructose-H_2O)$^-$ ions. The parent anion fructose$^-$ is readily observed with both Al (Al_2O_3) and Zn substrates, but each substrate presents different conformational components. The fructose$^-$ anion is not observed with either a filter paper or a Cu substrate. (Fructose-OH)$^-$ is only observed employing an RG6 matrix with a Cu substrate. An Au substrate is also considered; however, no uniquely identifiable fragment species or parent anion can be observed with an Au metal surface coupled with the MALDI process. Different properties of the substrates are explored and compared, including electron affinity of the metal atom, work function of the solid, and surface structure, composition, and chemistry: a Zn substrate has the lowest work function and a negative electron affinity. As such, Zn may produce more electrons during the MALD/ablation process and thereby generate more fructose related anion species.

(3) Possible reaction pathways for the formation of various observed fructose related anionic species are determined.

(Fructose-H)$^-$ and (fructose-OH)$^-$ are more likely already present in the beam after laser ablation. (Fructose-H_2O)$^-$ can be generated either from the ablation process or from both anionic and neutral reaction pathways from parent anions or neutrals by losing one H_2O molecule directly.

Additional molecular mechanisms or reaction channels for the generation of particular fructose related anions through potential energy surface calculations with reaction intermediates and transition states are being pursued. Also, the reaction pathways from cyclic structures to open chain structures for fructose related species will be considered and investigated. Subsequent investigations of hydrated fructose anions will be reported in the near future. Such studies help to understand the interactions of saccharides with other molecules. Biologically relevant monosaccharides, including D-ribose and deoxyribose, are presently under investigation by techniques similar to those recounted here.

Conflicts of interest

There are no conflicts to declare.

Acknowledgements

References

1 H. Perreault and C. E. Costello, *J. Mass Spectrom.*, 1999, **34**, 184.

2 D. Garozzo, G. Impallomeni, E. Spina, B. N. Green and T. Hutton, *Carbohydr. Res.*, 1991, **221**, 253.

3 B. Stahl, M. Steup, M. Karas and F. Hillenkamp, *Anal. Chem.*, 1991, **63**, 1463.

4 B. Spengler, J. W. Dolce and R. J. Cotter, *Anal. Chem.*, 1990, **62**, 1731.

5 M. L. Coates and C. L. Wilkins, *Anal. Chem.*, 1987, **59**, 197.

6 R. E. March and C. J. Stadey, *Rapid Commun. Mass Spectrom.*, 2005, **19**, 805.

7 H. D. Beckey, *Int. J. Mass Spectrom. Ion Phys.*, 1969, **2**, 500.

8 H. Krone and H. D. Beckey, *Org. Mass Spectrom.*, 1969, **2**, 427.

9 H. R. Schulten, *Int. J. Mass Spectrom. Ion Phys.*, 1979, **32**, 97.

10 B. Mulroney, J. C. Traeger and B. A. Stone, *J. Mass Spectrom.*, 1995, **30**, 1277.

11 J.-C. Prome, H. Aurelle, D. Prome and A. Savagnac, *Org. Mass Spectrom.*, 1987, **22**, 6.

12 H. Egge and J. Peter-Katalinić, *Mass Spectrom. Rev.*, 1987, **6**, 331.

13 J. W. Dallinga and W. Heerma, *Biol. Mass Spectrom.*, 1991, **20**, 215.

14 V. N. Reinhold and S. A. Carr, *Mass Spectrom. Rev.*, 1983, **2**, 153.

15 R. B. Cole, J. C. Tabet, C. Salles, J. C. Jallageas and J. Crouzet, *Rapid Commun. Mass Spectrom.*, 1989, **3**, 59.

16 J. A. Carroll, L. Ngoka, C. G. Beggs and C. B. Lebrilla, *Anal. Chem.*, 1993, **65**, 1582.

17 S. Zapfe and D. Müller, *Rapid Commun. Mass Spectrom.*, 1998, **12**, 545.

18 N. C. Polfer, J. J. Valle, D. T. Moore, J. Oomens, J. R. Eyler and B. Bendiak, *Anal. Chem.*, 2006, **78**, 670.

19 J.-W. Shin and E. R. Bernstein, *J. Chem. Phys.*, 2014, **140**, 044330.

20 J.-W. Shin, F. Dong, M. E. Grisham, J. J. Rocca and E. R. Bernstein, *Chem. Phys. Lett.*, 2011, **506**, 161.

21 B. Spengler, D. Kirsch, R. Kaufmann and J. Lemoine, *Org. Mass Spectrom.*, 1994, **29**, 782.

23342 | *Phys. Chem. Chem. Phys.*, 2017, **19**, 23325–23344

This journal is © the Owner Societies 2017

22 I. Bald, H. D. Flosadóttir, J. Kopyra, E. Illenberger and O. Ingólfsson, *Int. J. Mass Spectrom.*, 2009, **280**, 190.

23 D. J. Harvey, *Mass Spectrom. Rev.*, 1999, **18**, 349.

24 H. D. Flosadottir, I. Bald and O. Ingólfsson, *Int. J. Mass Spectrom.*, 2011, **305**, 50.

25 D. J. Harvey, *Mass Spectrom. Rev.*, 2015, **34**, 268.

26 E. J. Cocinero and P. Çarçabal, in *Gas-Phase IR Spectroscopy and Structure of Biological Molecules*, ed. A. M. Rijs and J. Oomens, Springer International Publishing, Cham, 2015, p. 299, , DOI: 10.1007/128_2014_596.

27 F. O. Talbot and J. P. Simons, *Phys. Chem. Chem. Phys.*, 2002, **4**, 3562.

28 R. A. Jockusch, F. O. Talbot and J. P. Simons, *Phys. Chem. Chem. Phys.*, 2003, **5**, 1502.

29 R. A. Jockusch, R. T. Kroemer, F. O. Talbot, L. C. Snoek, P. Çarçabal, J. P. Simons, M. Havenith, J. M. Bakker, I. Compagnon, G. Meijer and G. von Helden, *J. Am. Chem. Soc.*, 2004, **126**, 5709.

30 R. A. Jockusch, R. T. Kroemer, F. O. Talbot and J. P. Simons, *J. Phys. Chem. A*, 2003, **107**, 10725.

31 P. Çarçabal, R. A. Jockusch, I. Hünig, L. C. Snoek, R. T. Kroemer, B. G. Davis, D. P. Gamblin, I. Compagnon, J. Oomens and J. P. Simons, *J. Am. Chem. Soc.*, 2005, **127**, 11414.

32 E. Cristina Stanca-Kaposta, D. P. Gamblin, J. Screen, B. Liu, L. C. Snoek, B. G. Davis and J. P. Simons, *Phys. Chem. Chem. Phys.*, 2007, **9**, 4444.

33 N. A. Macleod, C. Johannessen, L. Hecht, L. D. Barron and J. P. Simons, *Int. J. Mass Spectrom.*, 2006, **253**, 193.

34 J. Screen, E. C. Stanca-Kaposta, D. P. Gamblin, B. Liu, N. A. Macleod, L. C. Snoek, B. G. Davis and J. P. Simons, *Angew. Chem., Int. Ed.*, 2007, **46**, 3644.

35 E. J. Cocinero, E. C. Stanca-Kaposta, E. M. Scanlan, D. P. Gamblin, B. G. Davis and J. P. Simons, *Chem. – Eur. J.*, 2008, **14**, 8947.

36 E. B. Cagmat, J. Szczepanski, W. L. Pearson, D. H. Powell, J. R. Eyler and N. C. Polfer, *Phys. Chem. Chem. Phys.*, 2010, **12**, 3474.

37 S. E. Stefan and J. R. Eyler, *Int. J. Mass Spectrom.*, 2010, **297**, 96.

38 D. J. Brown, S. E. Stefan, G. Berden, J. D. Steill, J. Oomens, J. R. Eyler and B. Bendiak, *Carbohydr. Res.*, 2011, **346**, 2469.

39 S. E. Stefan, M. Ehsan, W. L. Pearson, A. Aksenov, V. Boginski, B. Bendiak and J. R. Eyler, *Anal. Chem.*, 2011, **83**, 8468.

40 E. J. Cocinero, A. Lesarri, P. Écija, F. J. Basterretxea, J.-U. Grabow, J. A. Fernández and F. Castaño, *Angew. Chem., Int. Ed.*, 2012, **51**, 3119.

41 E. J. Cocinero, A. Lesarri, P. Écija, Á. Cimas, B. G. Davis, F. J. Basterretxea, J. A. Fernández and F. Castaño, *J. Am. Chem. Soc.*, 2013, **135**, 2845.

42 C. Bermúdez, I. Peña, C. Cabezas, A. M. Daly and J. L. Alonso, *ChemPhysChem*, 2013, **14**, 893.

43 I. Peña, E. J. Cocinero, C. Cabezas, A. Lesarri, S. Mata, P. Écija, A. M. Daly, Á. Cimas, C. Bermúdez, F. J. Basterretxea, S. Blanco, J. A. Fernández, J. C. López,

F. Castaño and J. L. Alonso, *Angew. Chem., Int. Ed.*, 2013, **52**, 11840.

44 I. Pena, C. Cabezas and J. L. Alonso, *Chem. Commun.*, 2015, **51**, 10115.

45 J. L. Alonso, M. A. Lozoya, I. Pena, J. C. Lopez, C. Cabezas, S. Mata and S. Blanco, *Chem. Sci.*, 2014, **5**, 515.

46 C. Bermúdez, I. Peña, S. Mata and J. L. Alonso, *Chem. – Eur. J.*, 2016, **22**, 16829.

47 P. Sulzer, S. Ptasinska, F. Zappa, B. Mielewska, A. R. Milosavljevic, P. Scheier, T. D. Märk, I. Bald, S. Gohlke, M. A. Huels and E. Illenberger, *J. Chem. Phys.*, 2006, **125**, 044304.

48 S. Ptasińska, S. Denifl, S. Gohlke, P. Scheier, E. Illenberger and T. D. Märk, *Angew. Chem., Int. Ed.*, 2006, **45**, 1893.

49 S. Ptasińska, S. Denifl, P. Scheier and T. D. Märk, *J. Chem. Phys.*, 2004, **120**, 8505.

50 I. Bald, J. Kopyra and E. Illenberger, *Angew. Chem., Int. Ed.*, 2006, **45**, 4851.

51 H.-S. Im and E. R. Bernstein, *J. Chem. Phys.*, 2000, **113**, 7911.

52 S. Yin and E. R. Bernstein, *J. Chem. Phys.*, 2016, **145**, 154302.

53 B. Yuan, Z. Yu and E. R. Bernstein, *J. Chem. Phys.*, 2015, **142**, 124315.

54 Y. Yokoi, K. Kano, Y. Minoshima and T. Takayanagi, *Comput. Theor. Chem.*, 2014, **1046**, 99.

55 T. Fujita, M. Kondo and T. Takayanagi, *Comput. Theor. Chem.*, 2016, **1075**, 70.

56 N. A. Richardson, J. D. Gu, S. Y. Wang, Y. M. Xie and H. F. Schaefer, *J. Am. Chem. Soc.*, 2004, **126**, 4404.

57 P. Storoniak, J. Rak, Y. J. Ko, H. Wang and K. H. Bowen, *J. Chem. Phys.*, 2013, **139**, 075101.

58 J. L. Borioni, M. Puiatti, D. M. A. Vera and A. B. Pierini, *Phys. Chem. Chem. Phys.*, 2017, **19**, 9189.

59 P. Sarmah and R. C. Deka, *Mol. Simul.*, 2008, **34**, 879.

60 S. Kim and H. F. Schaefer III, *J. Chem. Phys.*, 2010, **133**, 144305.

61 M. Kobyłecka, J. Gu, J. Rak and J. Leszczynski, *J. Chem. Phys.*, 2008, **128**, 044315.

62 S. T. Stokes, A. Grubisic, X. Li, Y. J. Ko and K. H. Bowen, *J. Chem. Phys.*, 2008, **128**, 044314.

63 J. C. Rienstra-Kiracofe, G. S. Tschumper, H. F. Schaefer, S. Nandi and G. B. Ellison, *Chem. Rev.*, 2002, **102**, 231.

64 Z. Zeng and E. R. Bernstein, *J. Chem. Phys.*, 2016, **145**, 164302.

65 M. Rey, J. R. Aviles-Moreno and T. R. Huet, *Chem. Phys. Lett.*, 2006, **430**, 121.

66 L. M. Azofra, M. M. Quesada-Moreno, I. Alkorta, J. R. Aviles-Moreno, J. J. Lopez-Gonzalez and J. Elguero, *New J. Chem.*, 2014, **38**, 529.

67 B. Yuan and E. R. Bernstein, *J. Chem. Phys.*, 2017, **146**, 014301.

68 A. D. Becke, *J. Chem. Phys.*, 1993, **98**, 5648.

69 C. Lee, W. Yang and R. G. Parr, *Phys. Rev. B: Condens. Matter Mater. Phys.*, 1988, **37**, 785.

70 A. D. Becke, *Phys. Rev. A: At., Mol., Opt. Phys.*, 1988, **38**, 3098.

71 M. J. Frisch, G. W. Trucks, H. B. Schlegel, G. E. Scuseria, M. A. Robb, J. R. Cheeseman, G. Scalmani, V. Barone,

This journal is © the Owner Societies 2017

Phys. Chem. Chem. Phys., 2017, **19**, 23325–23344 | 23343

B. Mennucci, G. A. Petersson, H. Nakatsuji, M. Caricato, X. Li, H. P. Hratchian, A. F. Izmaylov, J. Bloino, G. Zheng, J. L. Sonnenberg, M. Hada, M. Ehara, K. Toyota, R. Fukuda, J. Hasegawa, M. Ishida, T. Nakajima, Y. Honda, O. Kitao, H. Nakai, T. Vreven, J. A. Montgomery Jr., J. E. Peralta, F. Ogliaro, M. Bearpark, J. J. Heyd, E. Brothers, K. N. Kudin, V. N. Staroverov, R. Kobayashi, J. Normand, K. Raghavachari, A. Rendell, J. C. Burant, S. S. Iyengar, J. Tomasi, M. Cossi, N. Rega, J. M. Millam, M. Klene, J. E. Knox, J. B. Cross, V. Bakken, C. Adamo, J. Jaramillo, R. Gomperts, R. E. Stratmann, O. Yazyev, A. J. Austin, R. Cammi, C. Pomelli, J. W. Ochterski, R. L. Martin, K. Morokuma, V. G. Zakrzewski, G. A. Voth, P. Salvador, J. J. Dannenberg, S. Dapprich, A. D. Daniels, O. Farkas, J. B. Foresman, J. V. Ortiz, J. Cioslowski and D. J. Fox, *Gaussian 09, Revision A.02*, Gaussian, Inc., Wallingford CT, 2009.

72 Y. Zhao and D. G. Truhlar, *Theor. Chem. Acc.*, 2008, **120**, 215.

73 Y. Zhao and D. G. Truhlar, *Acc. Chem. Res.*, 2008, **41**, 157.

74 A. Austin, G. A. Petersson, M. J. Frisch, F. J. Dobek, G. Scalmani and K. Throssell, *J. Chem. Theory Comput.*, 2012, **8**, 4989.

75 G. Banfalvi, *DNA Cell Biol.*, 2006, **25**, 189.

76 P. Dais and A. S. Perlin, *Carbohydr. Res.*, 1985, **136**, 215.

77 W. Funcke, C. von Sonntag and C. Triantaphylides, *Carbohydr. Res.*, 1979, **75**, 305.

78 P. Dais and A. S. Perlin, *Carbohydr. Res.*, 1987, **169**, 159.

79 A. Allerhand and D. Doddrell, *J. Am. Chem. Soc.*, 1971, **93**, 2779.

80 T. Sommerfeld, *J. Chem. Phys.*, 2007, **126**, 124301.